



## The architecture of lipid droplets in the diatom *Phaeodactylum tricornutum*

Josselin Lupette<sup>a</sup>, Antoine Jaussaud<sup>a</sup>, Khawla Seddiki<sup>a,1</sup>, Christian Morabito<sup>a</sup>, Sabine Brugière<sup>b</sup>, Hubert Schaller<sup>c</sup>, Marcel Kuntz<sup>a</sup>, Jean-Luc Putaux<sup>d</sup>, Pierre-Henri Jouneau<sup>e</sup>, Fabrice Rébeillé<sup>a</sup>, Denis Falconet<sup>a</sup>, Yohann Couté<sup>b</sup>, Juliette Jouhet<sup>a</sup>, Marianne Tardif<sup>b</sup>, Juliette Salvaing<sup>a</sup>, Eric Maréchal<sup>a,\*</sup>

<sup>a</sup> Laboratoire de Physiologie Cellulaire et Végétale, CNRS, CEA, INRA, Université Grenoble Alpes, Institut de Biosciences et Biotechnologies de Grenoble, CEA Grenoble, 17 avenue des Martyrs, 38000 Grenoble, France

<sup>b</sup> Laboratoire de Biologie à Grandes Echelles, Université Grenoble Alpes, CEA, Inserm, Institut de Biosciences Biotechnologies de Grenoble, CEA Grenoble, 17 avenue des Martyrs, 38000 Grenoble, France.

<sup>c</sup> Institut de Biologie Moléculaire des Plantes, CNRS, 12 Rue du général Zimmer, 67084 Strasbourg Cedex, France.

<sup>d</sup> Centre de Recherches sur les Macromolécules Végétales (CERMAV), CNRS, Université Grenoble Alpes, 38000 Grenoble, France.

<sup>e</sup> Laboratoire d'Etudes des Matériaux par Microscopie Avancée, Institut Nanosciences et Cryogénie, Service de Physique des matériaux et Microstructures, CEA-Grenoble; 17 rue des Martyrs, 38000 Grenoble, France

### ARTICLE INFO

#### Keywords:

Diatoms  
*Phaeodactylum*  
Secondary plastid  
Lipid droplets  
Triacylglycerol  
Betaine lipid  
Carotenoids  
Histones

### ABSTRACT

Diatoms are a major phylum of phytoplankton biodiversity and a resource considered for biotechnological developments, as feedstock for biofuels and applications ranging from food, human health or green chemistry. They contain a secondary plastid limited by four membranes, the outermost one being connected with the endoplasmic reticulum (ER). Upon nitrogen stress, diatoms reallocate carbon to triacylglycerol storage inside lipid droplets (LDs). The comprehensive glycerolipid and sterol composition and the architecture of diatom LDs are unknown. In *Phaeodactylum tricornutum*, LDs are in contact with plastid, mitochondria and uncharacterized endomembranes. We purified LDs from nitrogen-starved *P. tricornutum* cells to high purity level (99 mol% triacylglycerol of total glycerolipids). We used the Stramenopile Lipid Droplet Protein (StLDP) as a previously validated marker for the identity of *P. tricornutum* LD. Amphipathic lipids surrounding LDs consist of a betaine lipid, diacylglycerylhydroxymethyltrimethyl- $\beta$ -alanine (0.4 mol%); sulfoquinovosyldiacylglycerol (0.35 mol%); phosphatidylcholine (0.15 mol%) and one sterol, brassicasterol. By contrast with whole cell extracts, the betaine lipid from LDs only contains eicosapentaenoic acid paired with palmitoleic or palmitolenic acids. This polar lipid composition suggests a budding of LDs from the cytosolic leaflet of the plastid outermost membrane. LD pigments reveal a specific accumulation of  $\beta$ -carotene. The LD proteome obtained from three independent biological replicates, based on stringent filtering of extracted data, and following subtraction of proteins downregulated by nitrogen starvation, highlights a core proteome of 86 proteins, including StLDP. LD-associated proteins suggest connections with vesicular trafficking (coatamer, clathrin), cytoskeleton, plastid and mitochondria. Unsuspected LD-associated function includes protein synthesis (ribosomes), folding (chaperones), posttranslational modifications and quality control (ubiquitination and ERAD pathway), possibly preparing translation of specific mRNAs. The detection of histone proteins, as previously demonstrated in drosophila embryo LDs, also suggests the storage of nucleosome components, preparing cell division and chromatin packaging, when cells are not stressed anymore.

### 1. Introduction

The biodiversity of phytoplankton is immense [1], ranging from cyanobacteria to photosynthetic eukaryotes that contain either a chloroplast inherited from a primary endosymbiosis, like in green algae,

[2–4] or a complex photosynthetic organelle inherited from a secondary endosymbiosis, like in heterokonts [5–7]. Diatoms represent one of the largest groups of heterokonts, dominating oceanic and fresh water ecosystems, and contributing significantly to biogeochemical cycles, both as primary producers at the basis of food webs and as

\* Corresponding author.

E-mail address: [eric.marechal@cea.fr](mailto:eric.marechal@cea.fr) (E. Maréchal).

<sup>1</sup> Present address: Proteomics Platform Center, Centre de recherche du CHU de Québec, Faculty of Medicine, Université Laval, Québec City, Québec, Canada.

carriers of carbon and silicon toward the ocean interior [8]. Diatoms have also attracted the attention as a promising resource for biotechnological developments, as feedstock for biofuels and applications ranging from food, human health or green chemistry [9–12]. In spite of their importance in eukaryote's evolution, role in ecosystems and potential for biotechnologies, knowledge of diatom subcellular architecture and physiology is still poor. Efforts need to be pursued, in such models as *Phaeodactylum tricornutum* [13–15].

Diatoms living in oceans and fresh waters are permanently exposed to environmental variations and stresses. Nutrient starvation [14,16,17], high temperature [18,19], high light [19], exposure to nitric oxide [20], to hydrogen peroxide [21–23] or to a variety of chemicals [24–27] are known to trigger an intense lipid remodeling marked by an accumulation of lipid droplets (LDs) within cells. The rationale for LD formation as part of general stress responses is not fully comprehended.

LDs are ubiquitously found in prokaryotic and eukaryotic cells [28–30]. Their architecture is based on a hydrophobic core containing neutral lipids, such as triacylglycerols (TAG), steryl esters, hydrophobic pigments etc. This core is surrounded by a monolayer of polar lipids, mainly phospholipids, with embedded or transiently associated proteins [28,31]. In our current understanding and based on works achieved on yeasts or mammals, the biogenesis of LDs occurs at the outer leaflet of the endoplasmic reticulum (ER) [28,32,33]. The proteome of nascent and budding LDs can therefore include (1) ER-located enzymes synthesizing neutral lipids, such as diacylglycerol acyltransferases (DGATs) or phosphatidylcholine:diacylglycerol acyltransferases (PDATs), (2) proteins involved in LD overall assembly like seipins, and (3) structural proteins stabilizing its sub-spherical shape and protecting its hydrophobic core. In more mature LDs, associated proteins can include (4) enzymes involved in the hydrolysis of neutral lipids, mainly TAG lipases, and conversion of fatty acids into other metabolites, as well as (5) proteins involved in the docking to the cytoskeleton and organelles, such as mitochondria or peroxisomes, or eventually (6) proteins involved in other functions [28,34,35]. In each environmental and physiological context, the function of the LD depends on its protein equipment [28,34,35]. The understanding of LD architecture and function requires therefore a precise inventory of its lipophilic and protein components.

LD-associated proteins are not conserved in evolution, and it is therefore necessary to determine the proteome of LDs in each major clade. Besides the differences, a structural classification of proteins has been proposed [36], with class I proteins having a hydrophobic 'hairpin' motif, such as plant oleosins, caleosin and stereoleosins [37,38], accessing LDs from the ER either during LD formation (budding) or after LD maturation via ER-LD membrane bridges. Class II proteins, such as mammal's perilipins [36,39], access the LD surface from the cytosol, binding to LDs through amphipathic helices or other hydrophobic domains. Additional proteins can also bind to LD following protein-protein interactions [36].

Proteomic analyses of nitrogen stress-induced LDs have been conducted in cells of Chlorophyta (green algae) containing a primary plastid, like *Chlamydomonas reinhardtii* [16,40,41], *Chlorella* sp. [42], *Haematococcus pluvialis* [43], three *Dunaliella* species [44], *Scenedesmus quadricauda* [45], or *Lobosphaera incisa* [46]. All these studies have highlighted the presence of major structural proteins. In some green algae like *Chlamydomonas*, an important set of enzymes involved in TAG formation was still associated to the mature LDs, as well as components of a multimeric ABC transporter of the chloroplast envelope involved in lipid transfers, suggesting a role of this organelle in providing precursors for some of the TAGs accumulating in LDs [16].

In diatoms, by contrast, the secondary plastid is delineated by four membranes and the outermost one is continuous with the nuclear envelope and therefore connected to the endomembrane system, including the ER [47] (Fig. 1). The outermost membrane of the plastid, or epiplastid membrane (EpM) [7] is therefore likely to share some

functions with the ER. The electron microscopy images of cells of the pennate diatom *P. tricornutum* shows tight connections between the LD and the EpM (LD-EpM contact sites), endomembrane vesicles (LD-endomembrane contact sites) and the mitochondria outer envelope membrane (LD-mitochondria contact sites) [47] (Fig. 1). It is not known whether the LD-EpM contact corresponds to a site of LD biogenesis, following the proposed model of LD-budding from the ER in mammal and yeast cells, or if it corresponds to independent functional interactions. Based on electron microscopy, it is not yet possible to determine whether endomembrane vesicles interacting with the LD correspond to the ER, peroxisomes or other compartments. LD-mitochondria contact sites are also observed [47] (Fig. 1), consistently with a docking to an organelle, where beta-oxidation of FAs could occur. The proteome of diatom LDs could possibly comprise proteins involved in these inter-organelle interactions.

Recent proteomic studies of nitrogen stress induced LDs in photosynthetic heterokonts have been performed in the pennate diatoms *Fistulifera solaris* [48] and *P. tricornutum* [49], allowing the identification of 15 and 5 putative LD proteins respectively, as well as in the eustigmatophyte *Nannochloropsis oceanica* [50]. These studies have mostly focused on the search for major structural proteins covering the surface of the LDs and ensuring its stability and controlling its size.

Here we addressed the architecture of the mature LD induced by nitrogen starvation, inside the cells of *P. tricornutum*. In LD-enriched fractions purified on a sucrose density gradient, five proteins have been previously described, i.e. a major Stramenopile LD Protein (StLDP - Phatr3\_J48859), an Acyl-CoA-binding protein (Phatr3\_J48778), a heat shock protein (HSP70 - Phatr3\_J54019) and two hypothetical proteins possibly involved in redox reactions (Phatr3\_J45894 and Phatr3\_J49981) [49]. The StLDP is a class I protein of 456 amino acids (49 kDa) having a hydrophobic domain of 54 amino acids (in position 222–275) forming a pattern X<sub>7</sub>PX<sub>9</sub>PX<sub>10</sub>PX<sub>3</sub>PX<sub>23</sub> (with P a proline) [49]. The expression of the *stldp* gene is upregulated upon nitrogen starvation [49].

The location of the StLDP at the LD has been confirmed based on GFP-fusion imaging [51]. The StLDP is therefore a validated marker of *Phaeodactylum* LD induced by nitrogen starvation. In the present study, we refined the method to prepare highly purified LDs from *P. tricornutum* cells and performed a comprehensive analysis of the lipids, pigments and proteome, allowing the characterization of LD components and revealing unsuspected roles.

## 2. Materials and methods

### 2.1. Cultivation of *Phaeodactylum tricornutum*

*Phaeodactylum tricornutum* (Pt1) Bohlin Strain 8.6 CCMP2561 (Culture Collection of Marine Phytoplankton, now known as NCMA: National Center for Marine Algae and Microbiota) was used in all experiments. Pt1 cells were maintained and grown in a volume of 1 L in 2-L flasks at 20 °C, in a modified ESAW (Enriched Seawater, Artificial Water) medium (NaCl 362.7 mM; Na<sub>2</sub>SO<sub>4</sub> 25 mM; KCl 8.03 mM; NaHCO<sub>3</sub> 2.067 mM; KBr 0.725 mM; H<sub>3</sub>BO<sub>3</sub> 0.372 mM; NaF 0.0657 mM; MgCl<sub>2</sub> 47.18 mM; CaCl<sub>2</sub> 9.134 mM; SrCl<sub>2</sub> 0.082 mM; Na<sub>2</sub>-glycerophosphate 21.8 μM; Na<sub>2</sub>SiO<sub>3</sub> 105.6 μM; disodium ethylenediaminetetraacetate dehydrate (Na<sub>2</sub>EDTA) 14.86 μM; Fe(NH<sub>4</sub>)<sub>2</sub>(SO<sub>4</sub>)<sub>2</sub> 5.97 μM; FeCl<sub>3</sub> 0.592 μM; MnSO<sub>4</sub> 2.42 μM; ZnSO<sub>4</sub> 0.254 μM; CoSO<sub>4</sub> 0.0569 μM; Na<sub>2</sub>MoO<sub>4</sub> 0.52 μM; H<sub>3</sub>BO<sub>3</sub> 61.46 μM; Na<sub>2</sub>SeO<sub>3</sub> 10 nM; biotin (vitamin H) 8.18 nM; cobalamin (vitamin B<sub>12</sub>) 2.94 nM; thiamine (vitamin B<sub>1</sub>) 0.594 μM [52] using ten times enriched nitrogen and phosphate sources (10N10P containing 5.49 mM NaNO<sub>3</sub> and 0.224 mM NaH<sub>3</sub>PO<sub>4</sub>) [14]. Nitrogen starvation was performed by transferring cells to the same medium without any addition of NaNO<sub>3</sub> (00N10P medium). Cells were grown on a 12:12 light (50 μE m<sup>-2</sup>sec<sup>-1</sup>) / dark cycle. Growth was evaluated by cell counting using a TECAN infinite M1000Pro plate reader and determined following the equation  $y = 1.834 \cdot 10^{-08}$

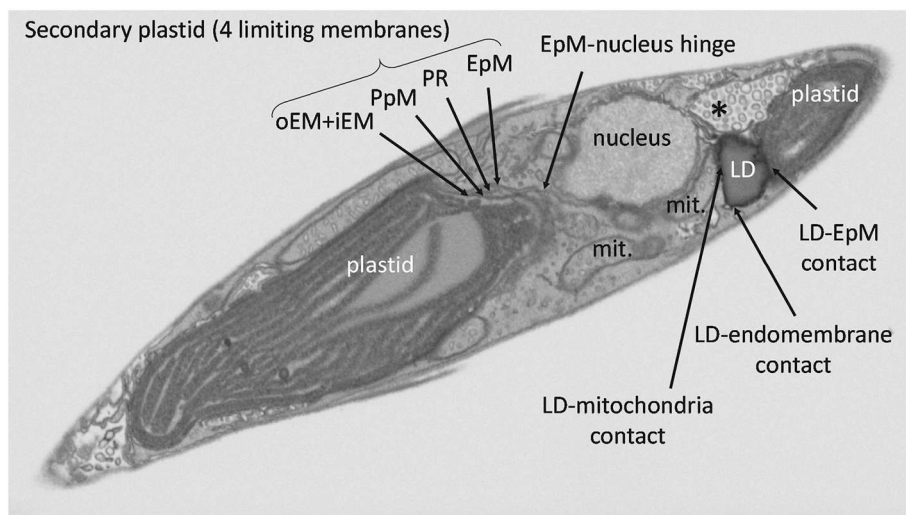


**Fig. 1.** Interactions of the lipid droplet of *P. tri-cornutum* with other organelles. Cells were collected in late exponential phase (beginning of nitrogen starvation). iEM, chloroplast inner envelope membrane; LD, lipid droplet; mit, mitochondria; PR, periplastid reticulum; PPM, periplastid membrane; oEM, chloroplast outer envelope membrane; EpM, epiplastid membrane; \*, an uncharacterized endomembrane compartment differing from the mitochondrion by the absence of an electron-dense matrix and the presence of vesicles inside a membrane sack.

$x + 0.03758$  with  $x$  = the absorbance at 730 nm and  $y$  = the number of cells [24].

## 2.2. Evaluation of neutral lipid accumulation by Nile red staining

Accumulation of triacylglycerol droplets was monitored by Nile Red (Sigma Aldrich) fluorescent staining as previously described [14,53]. In brief, cells were diluted and adjusted to a cell density that was linearly correlated with Nile Red fluorescence. Nile Red solution (40  $\mu$ L of a 2.5  $\mu$ g·mL<sup>-1</sup> stock solution in DMSO) was added to 160  $\mu$ L cell suspensions. LD stained with Nile Red were then visualized using a Zeiss LSM800 confocal laser scanning microscope equipped with a Zeiss Plan-APO x63-numerical aperture 1.46 oil immersion objective and enlarged x4. Nile Red fluorescence was monitored by excitation at 488 nm and capture zone ranging from 579 nm to 641 nm. Chlorophyll fluorescence was monitored by excitation at 488 nm and by capture zone ranging from 650 nm to 700 nm. Bright field acquisitions were also performed. Acquisition was saved under the Zeiss .czi format and imported with ImageJ 1.48v thanks to the BIO-FORMATS plugins 5.7.2. Alternatively, Nile red fluorescence values were normalized to the cell concentration.

## 2.3. Purification of lipid droplets

Lipid droplet (LD) purification was carried out in three independent biological replicates, from *P. tri-cornutum* cells cultivated in a 3-L volume (10N10P), up to a cell concentration of  $5 \times 10^6$  cells·mL<sup>-1</sup>, then subjected to nitrogen starvation (00N10P) for 7 days. Cells were collected by centrifugation at 6000  $\times$ g, 4 °C for 20 min (JLA 10.500 rotor, Beckman Coulter, Brea, CA, USA) and resuspended using a salt buffer (10 mM Tris-HCl + 2% NaCl). Cells were then collected by an additional centrifugation at 6000  $\times$ g, 4 °C for 20 min and resuspended in 50 mL of a sucrose buffer (sucrose 0.25 M; EDTA 1 mM; Tris-HCl 10 mM, final concentration, pH 7.6) supplemented with a protease inhibitor cocktail (cOmplete, Roche Diagnostics). Concentrated cells were broken using a cell disruption systems (Constant Systems Limited, Daventry, UK) set at a 2 kbar rupture pressure. Cell breakage was verified by confocal imaging. Presence of LDs was assessed by Nile red staining as described above. The broken cells were centrifuged at 48,000  $\times$ g (JA 20 Rotor, Beckman Coulter, Brea, CA, USA), 4 °C for 20 min (SS34 rotor, Beckman Coulter, Brea, CA, USA) to eliminate the largest cell debris. The supernatant was recovered and adjusted to a concentration of sucrose 1.25 M. A cushion of 4.5 mL of this fraction was loaded at the bottom of an ultracentrifuge tube (SW32ti, Beckman Coulter, Brea, CA, USA). A second layer of 7 mL sucrose 0.7 M; Triton X-100 0.2% v/v; Tris-HCl 10 mM pH 7.6 supplemented with a protease

inhibitor cocktail was added gently above the sample. A third layer of 1.5 mL sucrose 0.25 M; Tris-HCl 10 mM pH 7.6 supplemented with protease inhibitor cocktail was added gently on top of the discontinuous gradient. Gradient was ultracentrifuged at 68,000  $\times$ g, 4 °C for 16 h. LDs were carefully collected at the top of the tubes and transferred into 1.5 mL tubes. LDs were washed two times in Tris-HCl 10 mM, pH 7.6 at 20,000  $\times$ g, 4 °C for 10 min (S55A2 Rotor, Hitachi Koki, Tokyo, Japan). A volume of 6.85 mL of purified LD is obtained per purification. The enrichment in LDs was controlled in an aliquot fraction by confocal imaging, fixed in 3% agarose in Tris-HCl 10 mM pH 7.6 in order to limit LD movements.

## 2.4. Sample preparation for lipidomic and proteomic analyses

Each sample corresponding to whole cells and purified LDs were divided in fractions for lipidomic, pigment and proteomic analyses, respectively. For lipidomic analyses (glycerolipids, sterols, carotenoids), hydrophobic metabolites were extracted using solvents, either from freeze-dried cells corresponding to a 50 mL aliquot fraction of the nitrogen starved culture used for LD purification or from 850  $\mu$ L of purified LD fractions. Whole cell lipids were extracted using the Folch method [54,55]. In brief, freeze-dried cells were suspended in 4 mL of boiling ethanol for 5 min to prevent lipid degradation, and lipids were extracted by addition of 2 mL methanol and 8 mL chloroform at room temperature. The mixture was then saturated with argon and stirred for 1 h at room temperature. After filtration through glass wool, cell debris were rinsed with 3 mL chloroform/methanol 2:1, v/v, and 5 mL of NaCl 1% were added to the filtrate to initiate phase separation. The chloroform phase was dried under argon before solubilizing the lipid extract in 1 mL of chloroform. LD lipids were extracted using the Bligh and Dyer method [14,56]. Extracted lipids were dried under a flow of argon and conserved at -20 °C until analyses. For proteomic analyses, proteins from purified LDs were precipitated overnight at -20 °C in cold acetone. Samples were centrifuged at 20,000  $\times$ g (S55A2 Rotor, Hitachi Koki, Tokyo, Japan), 0 °C for 10 min. The supernatant was discarded and the pellet was incubated at -20 °C in cold ethyl acetate for 2 h to eliminate residual oil. Samples were centrifuged at 20,000  $\times$ g, 0 °C for 10 min. The supernatant was discarded and the pellet was dried under a fume hood to remove traces of ethyl acetate. Three independent purifications were performed, corresponding to biological replicates. For each independent purification, LD proteins were suspended in 100  $\mu$ L of a lysis buffer (urea 7 M, thiourea 2 M, 3-((3-cholamidopropyl) dimethylammonio)-1-propanesulfonate (CHAPS) 4% w/v, Triton X-100 3% v/v and SDS 2% w/v). The quantity of purified LD proteins was evaluated on 2  $\mu$ L aliquots, loaded onto a SDS PAGE and stained using



the SilverQuest staining kit (Invitrogen, Carlsbad, CA, USA) in comparison with known amounts of proteins from a whole cell fraction resolved in parallel. 8  $\mu\text{L}$  of purified LD proteins were used for proteomic analyses. The remaining fractions (86  $\mu\text{L}$  per independent purification, pooled in 258  $\mu\text{L}$ ) were concentrated using Ultracel - 3K filters (Merck Millipore Ltd., Tullagreen, Carrigtwohill, Ireland), and eluted in a final volume of 48  $\mu\text{L}$ , used for further SDS PAGE and Western blot analyses.

## 2.5. Glycerolipid profiling by liquid chromatography - tandem mass spectrometry

For each whole cell and LD lipid extracts, total glycerolipids were quantified from their fatty acids (FAs): in a 10  $\mu\text{L}$  aliquot fraction a known quantity of saturated 15-carbon FA (15:0) was added and all FAs were methanolized into methyl esters (FAME) by a 1 h incubation in 3 mL 2.5%  $\text{H}_2\text{SO}_4$  in pure methanol at 100 °C [57]. The reaction was stopped by addition of 3 mL water, and 3 mL hexane was added for phase separation. After 20 min of incubation, the hexane phase was transferred to a new tube. FAMES were extracted a second time via the addition, incubation and extraction of another 3 mL hexane. The combined collected hexane fractions (6 mL) were argon-dried and FAMES were suspended in 40  $\mu\text{L}$  hexane for analysis by gas chromatography coupled with flame ionization detection (GC-FID) (Perkin Elmer), using a BPX70 (SGE) column. FAMES were identified by comparison of their retention times with those of standards (Sigma) and quantified by the surface peak method using 15:0 for calibration. Extraction and quantification were performed with three biological replicates. Glycerolipids were then analyzed and quantified by high-pressure liquid chromatography-tandem mass spectrometry (HPLC-MS/MS), with appropriate standard lipids [58]. In brief, lipid extracts corresponding to 25 nmol of total fatty acids were dissolved in 100  $\mu\text{L}$  of chloroform/methanol [2/1, v/v] containing 125 pmol of each internal standard. Internal standards used were phosphatidylethanolamine (PE) 18:0–18:0 and diacylglycerol (DAG) 18:0–22:6 from Avanti Polar Lipid, and sulfoquinovosyldiacylglycerol (SQDG) 16:0–18:0 extracted from spinach thylakoid [59] and hydrogenated [60]. Lipids were then separated by HPLC and quantified by MS/MS. Lipid classes were separated using an Agilent 1200 HPLC system using a 150 mm  $\times$  3 mm (length  $\times$  internal diameter) 5  $\mu\text{m}$  diol column (Macherey-Nagel), at 40 °C. The mobile phases consisted of hexane/isopropanol/water/1 M ammonium acetate, pH 5.3 [625/350/24/1, v/v] (A) and isopropanol/water/1 M ammonium acetate, pH 5.3 [850/149/1, v/v] (B). The injection volume was 20  $\mu\text{L}$ . After 5 min, the percentage of B was increased linearly from 0 to 100% in 30 min and kept at 100% for 15 min. This elution sequence was followed by a return to 100% A in 5 min and an equilibration for 20 min with 100% A before the next injection, leading to a total runtime of 70 min. The flow rate of the mobile phase was 200  $\mu\text{L}/\text{min}$ . The distinct glycerophospholipid classes were eluted successively as a function of the polar head group. Mass spectrometric analysis was performed on a 6460 triple quadrupole mass spectrometer (Agilent) equipped with a Jet stream electrospray ion source under following settings: drying gas heater at 260 °C, drying gas flow at 13  $\text{L}\cdot\text{min}^{-1}$ , sheath gas heater at 300 °C, sheath gas flow at 11  $\text{L}\cdot\text{min}^{-1}$ , nebulizer pressure at 25 psi, capillary voltage at  $\pm$  5000 V and nozzle voltage at  $\pm$  1000 V. Nitrogen was used as collision gas. The quadrupoles Q1 and Q3 were operated at widest and unit resolution respectively. Phosphatidylcholine (PC) and diacylglycerol hydroxymethyltrimethyl- $\beta$ -alanine (DGTA) analyses were carried out in positive ion mode by scanning for precursors of  $m/z$  184 and 236 respectively at a collision energy (CE) of 34 and 52 eV. SQDG analysis was carried out in negative ion mode by scanning for precursors of  $m/z$  -225 at a CE of -56 eV. Phosphatidylethanolamine (PE), phosphatidylinositol (PI), phosphatidylglycerol (PG), monogalactosyldiacylglycerol (MGDG) and digalactosyldiacylglycerol (DGDG) measurements were performed in positive ion mode by scanning for neutral losses of 141 Da, 277 Da, 189 Da, 179 Da and 341 Da at

CEs of 20 eV, 12 eV, 16 eV, 8 eV and 8 eV, respectively. DAG and triacylglycerol (TAG) species were identified and quantified by multiple reaction monitoring (MRM) as singly charged ions  $[\text{M} + \text{NH}_4]^+$  at a CE of 16 and 22 eV respectively. Quantification was done for each lipid species by multiple reaction monitoring (MRM) with 50 ms dwell time with the various transitions previously recorded [14]. Mass spectra were processed using the MassHunter Workstation software (Agilent) for identification and quantification of lipids. Lipid amounts (pmol) were corrected for response differences between internal standards and endogenous lipids and by comparison with a qualified control (QC). QC extract correspond to a known *P. tricornutum* lipid extract qualified and quantified by thin-layer chromatography and gas-chromatography coupled to ion flame detection as described previously [14].

## 2.6. Pigment extraction and HPLC analysis

Total pigments were analyzed either from *P. tricornutum* whole cells or from purified LDs. After collection by centrifugation at 11,000  $\times$ g, 4 °C, for 5 min,  $1.5 \times 10^8$  cells of *P. tricornutum* were resuspended in 100  $\mu\text{L}$  of cold Methanol - Tris-HCl (10 mM pH 7.4). Pigments were extracted under argon, on ice and in the dark. After centrifugation at 11,000  $\times$ g, 4 °C for 5 min, the supernatant was recovered, kept in the dark at 4 °C, and the pellet was further extracted 3 times with methanol 100%, i.e., until the pellet became white. All supernatant fractions were pooled together and dried under argon. Pigments from LDs were collected in the lipid fraction. Pigments from total extracts and LD fractions were resuspended in 100  $\mu\text{L}$  of dimethylformamide before injection on a HPLC (Varian ProStar 800, Walnut Creek, CA, USA) coupled to a diode array detector. The carotenoids were separated on a C18 reverse-phase column (250  $\times$  4.6 mm) manufactured by Macherey-Nagel using the following method. The initial mobile phase was methanol 80%/ammonium acetate 0.5 M 20%, followed by a linear gradient to 100% of a solvent B consisting of acetonitrile 90%/water 10% during 4 min, in turn followed by a linear gradient to 80% ethyl acetate/20% B up to 20 min, a solvent composition kept for another 5 min. Identification of carotenoids was achieved by comparing retention times and spectral properties acquired on-line with authentic standards (Fucoxanthin,  $\beta$ -carotene, lycopene).

## 2.7. Sterol analysis

Pure LD lipids were dissolved in 500  $\mu\text{L}$  benzene and stored at -20 °C. Aliquots (1/10 by volume) were used as test samples to evaluate the total ion chromatograms in gas chromatography coupled to mass spectrometry (GC-MS). Samples were treated by halves as follows, to determine both esterified and free sterols. Dried extracts were saponified in 300  $\mu\text{L}$  of KOH 6% in MeOH, for 1 h at 70 °C. Water (0.5 volume) was added to the mixture. The non-saponifiable compounds were extracted with three volumes of *n*-hexane. The dried residue was acetylated in toluene (100  $\mu\text{L}$ ) in the presence of acetic anhydride (50  $\mu\text{L}$ ) and pyridine (40  $\mu\text{L}$ ) at 70 °C for 1 h. Reagents were air-dried (warm air stream) then the extract was dissolved in *n*-hexane (100 to 300  $\mu\text{L}$ ) in GC vials (with inserts). Alternatively, dried extracts were separated on thin layer chromatography (TLC) plates (Merck 60F<sub>254</sub>) using dichloromethane as a developing solvent. One run of TLC yielded resolved fractions of free sterols at  $R_f$  = 0.14 and at sterol esters (of fatty acids) at  $R_f$  = 0.86. Commercial cholesterol and cholesterol oleate were used as TLC standards. Fractions containing free sterols and sterol esters were scrapped off the plate. Sterol esters were saponified as described above. Residues were then acetylated and analyzed by GC-MS. The temperature program of the oven of an Agilent 6890 chromatograph coupled to an Agilent 5973 mass selective detector included a steep ramp from 60 to 220 °C (30 °C $\cdot$ min<sup>-1</sup>) then a 2 °C $\cdot$ min<sup>-1</sup> ramp from 220 to 300 °C, followed by a 10 min plateau. Compounds were separated on a HP5-MS column (Agilent; 30 m long, 0.32 mm i.d., 0.25 mm film thickness; 2  $\text{mL}\cdot\text{min}^{-1}$  hydrogen as carrier gas) and

identified by their mass spectra. Brassicasteryl acetate was detected at  $R_t = 34.5$  min, its mass spectrum at EI 70 eV [ $M^+ - ROH$  380(100),  $M^+ - CH_3 - ROH$  365(5),  $M^+ - SC - ROH$  255(25)] and retention time was identical to that of an authentic standard. Total brassicasterol acetate in extracts was determined according to a standard curve.

## 2.8. Proteomic analyses

### 2.8.1. SDS-PAGE and in-gel trypsin digestion

LD fractions were prepared in biological triplicate. 8  $\mu$ L of purified LD proteins adjusted to 25  $\mu$ L Laemmli buffer were loaded on top of a SDS-PAGE gel (NuPAGE 4–12%, Invitrogen) and migrated on a 60 mm distance in order to separate potential lipidic front from the protein content. After Coomassie blue staining (R250, Bio-Rad), the gel areas containing proteins were manually excised and cut into 8 bands for in-gel digestion with trypsin using a Freedom EVO150 robotic platform (Tecan Trading AG, Switzerland) as follows. Gel bands were washed six times by successive incubations in  $NH_4HCO_3$  25 mM and then in  $CH_3CN$  50% v/v,  $NH_4HCO_3$  25 mM. After dehydration in pure  $CH_3CN$ , reduction was carried out with DTT 10 mM in  $NH_4HCO_3$  25 mM (45 min at 53 °C) and alkylation with iodoacetamide 55 mM in  $NH_4HCO_3$  25 mM (35 min in the dark). Alkylation was stopped by the addition of DTT 10 mM in  $NH_4HCO_3$  25 mM (10-min incubation). Gel pieces were then washed again in  $NH_4HCO_3$  25 mM and dehydrated with pure acetonitrile. Modified trypsin (sequencing grade, Promega) in  $NH_4HCO_3$  25 mM was added to the dehydrated gel pieces for incubation at 37 °C overnight. Peptides were extracted from gel pieces in three sequential extraction steps (each 15 min) in 30  $\mu$ L of  $CH_3CN$  50% v/v, 30  $\mu$ L of formic acid 5% v/v, and finally 30  $\mu$ L of pure  $CH_3CN$ . The pooled supernatants were dried under vacuum.

### 2.8.2. Analysis of trypsin peptides by nanoliquid chromatography coupled to tandem mass spectrometry (nanoLC-MS/MS)

The dried extracted peptides were resuspended in acetonitrile 5%, trifluoroacetic acid 0.1% and analyzed via online nano-LC-MS/MS (nano-liquid chromatography-tandem mass spectrometry; NCS and Q-Ex HF, Thermo Fischer Scientific). Peptide mixtures were desalted on line using a reverse phase precolumn (Reprosil PUR C18 AQ 1.9  $\mu$ m, 250 mm  $\times$  75  $\mu$ m; Cluzeau) and resolved on a C18 column (Acclaim PepMap 100 C18, 3  $\mu$ m bead size, 100 Å pore size, 250 mm  $\times$  75  $\mu$ m, Dionex). Peptides were separated using 140-min gradients ranging from 4% to 50% acetonitrile in formic acid 0.1% in 123 min and wash to 90% and equilibration at 4% at a flow rate of 300 nL·min<sup>-1</sup>. MS (mass spectrometry) and MS/MS data were acquired using the Xcalibur software (Thermo Fisher Scientific). The spray voltage was set at 2 kV and the heated capillary was adjusted to 270 °C. Survey full-scan MS spectra ( $m/z = 400$ –1600) were obtained in the Orbitrap with a resolution of 60,000 after accumulation of  $1.10^6$  ions (maximum filling time: 200 ms). The 20 most intense ions from the preview survey scan delivered by the Orbitrap were fragmented via collision-induced dissociation in the LTQ after accumulation of  $1^{e5}$  ions (maximum filling time: 50 ms). Raw files were processed using MaxQuant version 1.5.8.3 [61].

### 2.8.3. Protein determination

Mass spectrometry spectra were searched against a compilation of the *P. tricornutum* protein database from the Ensembl Protists portal (Phaeodactylum\_tricornutum.ASM15095v2.pep.all.fasta, 12,178 entries), the organellar-encoded proteins (165 entries) and the frequently observed contaminant database embedded in MaxQuant. Trypsin/P was chosen as the enzyme and 2 missed cleavages were allowed. Precursor mass error tolerances were set respectively at 20 ppm and 4.5 ppm for first and main searches. Fragment mass error tolerance was set to 20 ppm. Peptide modifications allowed during the search were: carbamidomethylation (C, fixed), acetyl (Protein N-ter, variable), and oxidation (M, variable). Minimum peptide length was set to 7 amino acids.

Minimum number of peptides, razor + unique peptides and unique peptides were all set to 1. Maximum false discovery rates, calculated by employing a reverse database strategy, were set to 0.01 at peptide and protein levels. For quantification, the “Match between runs” option was activated. To evaluate the relative abundance of each protein in the LDs preparations, proteins were quantified using iBAQ [62]. Proteins that failed to be quantified in all three replicates were discarded. iBAQ values were normalized to the sum of all intensities within each replicate. Proteins were ranked according to the sum of normalized iBAQ (decreasing order) thus including missing values with iBAQ = 0. For annotations: descriptions of the proteins were obtained from the Ensembl fasta file. This functional annotation was completed by expert annotations obtained from the corresponding gene version at JGI (<https://genome.jgi.doe.gov/Phatr2> and [https://genome.jgi.doe.gov/Phatr2\\_bd](https://genome.jgi.doe.gov/Phatr2_bd)), based on the search for signal peptides, using the SignalP predictive method [63], chloroplast transit peptides, based on the ChloroP predictive method [64] and on the detection of an ASAFAP-motif specific to sequence import into secondary plastids [65]. Prediction of transmembrane helices in proteins was performed at the TMHMM Server v. 2.0 (<http://www.cbs.dtu.dk/services/TMHMM-2.0>) [66] and isoelectric point (IP) values were predicted using the Avg\_Pi output of the standalone IPC Isoelectric Point Calculator program (<http://isoelectric.ovh.org/>) [67].

## 2.9. Western blot analyses

Immunodetection of organellar protein markers was performed on protein extracts from whole cells of *P. tricornutum* grown in nitrogen-rich and nitrogen-depleted media and from purified LD fractions. For whole cell extracts, 200 mL of *P. tricornutum* cells were either cultivated 7 days in 10N10P ESAW medium up to a cell concentration of  $8 \times 10^6$  cells·mL<sup>-1</sup> or incubated 7 days in 00N10P ESAW medium, after a 10-day growth in rich medium, up to a cell concentration of  $9.10^6$  cells·mL<sup>-1</sup>. Cells were collected by centrifugation at 4000  $\times$  g, 4 °C for 7 min (Rotor A-4-44, Eppendorf). Pellets were quickly frozen in liquid nitrogen and stored at -80 °C. Pellets were lyophilized and phenol extracted as described previously [68] with the addition of EDTA 50 mM,  $\beta$ -mercaptoethanol 2% v/v, PMSF 2 mM, and cOmplete protease inhibitor cocktail as specified by the supplier (Roche Diagnostics). A total of 15  $\mu$ g of proteins from whole cell extracts and of 2  $\mu$ g proteins from LDs were then resolved by SDS-PAGE on a 12% acrylamide gel before transfer to a nitrocellulose membrane. Immunodetection was performed by peroxidase-coupled detection (Clarity western ECL Substrate, Biorad). Antibodies against StLDP, Seipin, CNX, COP1, PEX3, ACL1, CGI-58, RAE1 and TPT1 were obtained by rabbit immunization (Biotem). Antibodies were affinity purified on the peptides. The purity of LD fraction was also checked with commercial antibody (Agriser): Sec21p (AS08 327), PsaC (AS10 939), PsaA (AS05 084) and ATP $\beta$  mitochondrial and chloroplastic (AS05 085). All the antibodies were used at a dilution of 1/1000 with the exception of CNX at 1/5000 and ATP $\beta$  at 1/2000.

## 2.10. Transmission electron microscopy

For whole cell imaging, cells of *P. tricornutum* were harvested at late logarithmic phase ( $2 \times 10^6$  cells·mL<sup>-1</sup>) before the offset of the light period, by centrifugation at 5000  $\times$  g, 4 °C for 10 min. Cells were then fixed in glutaraldehyde 2.5% (TAAB); formaldehyde 2% (Polysciences); cacodylate 0.1 M (Sigma-Aldrich), pH 7.4, for 1 h at room temperature. Electron microscopy observation was performed using a Zeiss NVision 40 dual-beam microscope as described previously [47,69]. For lipid droplet imaging, diluted suspensions of purified fractions were deposited onto glow-discharged carbon-coated TEM grids. After a few minutes, the liquid in excess was blotted with filter paper and, prior to drying, the preparation was negatively stained with 2% uranyl acetate. The stain in excess was blotted and the specimen was allowed to dry.

Images were recorded with a Philips-FEI CM200 microscope operating at 200 kV and equipped with a TVIPS TemCam F216 digital camera.

### 2.11. Statistical analysis

All the analytical determinations were performed in biological triplicate. Statistical analyses were achieved using GraphPad prism software (GraphPad software Inc., CA, USA). One-way and two-way ANOVA followed by Dunnett's post hoc test was carrying out. The difference between groups was considered significant when the *p*-value was equal to or < 0.05.

### 2.12. Accession numbers

Phatr3\_draftJ1735; Phatr3\_draftJ977; Phatr3\_EG00979; Phatr3\_EG01955; Phatr3\_EG01984; Phatr3\_EG02298; Phatr3\_EG02301; Phatr3\_EG02323; Phatr3\_EG02389; Phatr3\_EG02643; Phatr3\_J13587; Phatr3\_J13662; Phatr3\_J13951; Phatr3\_J14618; Phatr3\_J14792; Phatr3\_J15138; Phatr3\_J15806; Phatr3\_J17545; Phatr3\_J1884; Phatr3\_J20657; Phatr3\_J20885; Phatr3\_J21122; Phatr3\_J21239; Phatr3\_J21929; Phatr3\_J22006; Phatr3\_J22122; Phatr3\_J22357; Phatr3\_J22395; Phatr3\_J22873; Phatr3\_J24820; Phatr3\_J24978; Phatr3\_J25743; Phatr3\_J26290; Phatr3\_J26921; Phatr3\_J27118; Phatr3\_J27518; Phatr3\_J27976; Phatr3\_J28737; Phatr3\_J29260; Phatr3\_J29702; Phatr3\_J30315; Phatr3\_J30486; Phatr3\_J30519; Phatr3\_J30660; Phatr3\_J34971; Phatr3\_J35766; Phatr3\_J40880; Phatr3\_J41856; Phatr3\_J42434; Phatr3\_J44488; Phatr3\_J45510; Phatr3\_J45679; Phatr3\_J45813; Phatr3\_J46098; Phatr3\_J46448; Phatr3\_J48778; Phatr3\_J48859; Phatr3\_J49286; Phatr3\_J49287; Phatr3\_J4937; Phatr3\_J49943; Phatr3\_J50214; Phatr3\_J50215; Phatr3\_J50236; Phatr3\_J50705; Phatr3\_J50872; Phatr3\_J51058; Phatr3\_J51066; Phatr3\_J51128; Phatr3\_J51157; Phatr3\_J51230; Phatr3\_J51305; Phatr3\_J54019; Phatr3\_J54086; Phatr3\_J54360; Phatr3\_J54534; Phatr3\_J54642; Phatr3\_J54686; Phatr3\_J55010; Phatr3\_J55230; Phatr3\_J6847.

## 3. Results

### 3.1. Lipid droplet purification

LDs were purified from *P. tricornutum* wild-type cells (CCMP632/CCAP 1055/1; Pt1) cultivated in 3-liter batches in a rich medium (ESAW 10N10P) and subjected to a starvation in nitrogen (ESAW 00N10P) during seven days (Fig. 2, A1). Nitrogen starvation triggered the accumulation of LD within cells (Fig. 2, B1). We first sought to optimize the LD purification procedure previously described [49] so as to avoid contaminations by cellular debris. Cells were broken gently using a cell disruptor set at a pressure of 2 kbar. In confocal microscopy, Nile red-stained LDs appeared mixed with cell debris, including broken chloroplasts, assessed by chlorophyll fluorescence (Fig. 2A2 and B2). We then repeated the purification procedure described previously [49], by adjusting the sucrose concentration of the broken cells to 0.25 M, loading this sample on top of a 0.7 M sucrose cushion and proceeding with an ultracentrifugation at 50,000 ×g for 20 min at 4 °C. The SDS PAGE analysis of the obtained fraction showed a profile similar to that described by Yoneda et al. (2016). Nevertheless, LD collected at the upper surface of the tubes were not totally separated from lower density cell debris, as lipidomic profile indicated a strong contamination by MGDG and proteomic analyses returned > 1800 proteins in this fraction (data not shown). We sought therefore to improve this purification method, by loading the broken cell sample at the bottom of the density gradient [70,71]. We adjusted the sucrose concentration to 1.25 M, and loaded this sample (4.5 mL) under a discontinuous gradient made of 0.7 M (7 mL) and 0.25 M sucrose (1.5 mL) layers (Fig. 2A3). The fractionation was then achieved based on the buoyancy of low-density LDs. The 0.7 M layer also contained Triton-X100 so as to wash the surface of

LDs, while moving toward the upper surface of the discontinuous gradient. After a 16-hour ultracentrifugation at 68,000 ×g at 4 °C, LDs were collected at the surface of the tubes, clearly separated from higher density debris (Fig. 2A3). LD enrichment was monitored after cell disruption and after ultracentrifugation by confocal microscopy, based on Nile red staining (Fig. 2B3). Electron microscopy negative staining of purified LDs showed exclusively spherical structures with diameters of ~100–300 nm (Fig. 2C). This LD purification procedure was therefore used for three independent replicates and obtained LD fractions were used for further analyses.

### 3.2. Glycerolipidome of *P. tricornutum* lipid droplets

The glycerolipid composition of purified LDs was compared to the whole-cell glycerolipidome determined from *P. tricornutum* grown in nitrogen starvation (Fig. 3). Starved cells contained about 27 mol% of TAG, consistently with previous works [14,17]. Most abundant polar lipids were three plastid glycolipids, i.e. monogalactosyldiacylglycerol (MGDG, 43.8 mol%), digalactosyldiacylglycerol (DGDG, 11.7 mol%) and sulfoquinovosyldiacylglycerol (SQDG, 7.3 mol%). Phosphatidylcholine (PC, 5.5 mol%) and the betaine lipid diacylglycerolhydroxymethyl-*N,N,N*-trimethyl- $\beta$ -alanine (DGTA, 1.1 mol%) usually synthesized in the ER, were less abundant (Fig. 3A). The fraction of purified LDs contained 99.0% of TAG. MGDG represented < 0.05 mol% of LD lipids, confirming the high purity of the obtained fraction (Fig. 3A). No diacylglycerol could be detected in LDs (Fig. 3A) and the profile of TAG molecular species in the purified fraction was identical to that in whole cells (Fig. 3B), indicating that the integrity of LDs was not affected by lipases after cell breakage and separation on density gradient.

We detected DGTA (0.4 mol%), SQDG (0.35 mol%) and PC (0.15 mol%) in the LD (Fig. 3A). LDs contained nearly exclusively DGTA with eicosapentaenoic acid (C20:5) paired with palmitoleic or palmitolenic acids (C16:1 or C16:2), whereas whole cell DGTA contained also C16:0, all the C18:1, C18:2, C18:3 and C20:4 precursors of C20:5, as well as docosahexaenoic acid, C22:6 (Fig. 3C and D). PC and SQDG occurring in LD fractions had no significant difference in their fatty acid profiles compared to whole cell extracts (Fig. 3E and F). Whereas the presence of < 0.05% of the major plastid lipid, MGDG, indicated a remarkably low contamination by broken chloroplasts, the presence of SQDG indicates that this plastid lipid was specifically enriched at the surface of the LD.

### 3.3. A unique sterol in *P. tricornutum* lipid droplets, brassicasterol

Two major sterols have been previously identified in whole cells of *P. tricornutum*, i.e. brassicasterol (24-methylcholest-5,22-dien-3 $\beta$ -ol) and campesterol (24-methylcholest-5-en-3 $\beta$ -ol), with structures confirmed by mass spectrometry [72,73]. Brassicasterol and campesterol are structurally similar to cholesterol, containing 4 strongly hydrophobic hydrocarbon rings, a hydroxyl group at the 3-carbon atom of the A-ring and a short alkyl tail: these molecules display therefore amphipathic properties [74]. Here, we clearly identified one single molecular species, brassicasterol, in whole cells extracts and in purified LD fractions (Supplemental Fig. S1), representing < 5 mol% of total sterols + glycerolipids. Structure was assessed by mass spectrometry based on the identification of brassicasteryl specific fragments with *m/z* of 255.2 [M<sup>+</sup>-SC-ROH], 365.0 [3M<sup>+</sup>-CH3-ROH] and 380.4 [M<sup>+</sup>-ROH]. Remarkably, we could not detect any brassicasterol ester but only free brassicasterol as a pathway end-product. This low proportion of such an amphipathic lipid indicates that it is located close to, or inside the lipid monolayer at the surface of the LD and not in the hydrophobic core [75,76].

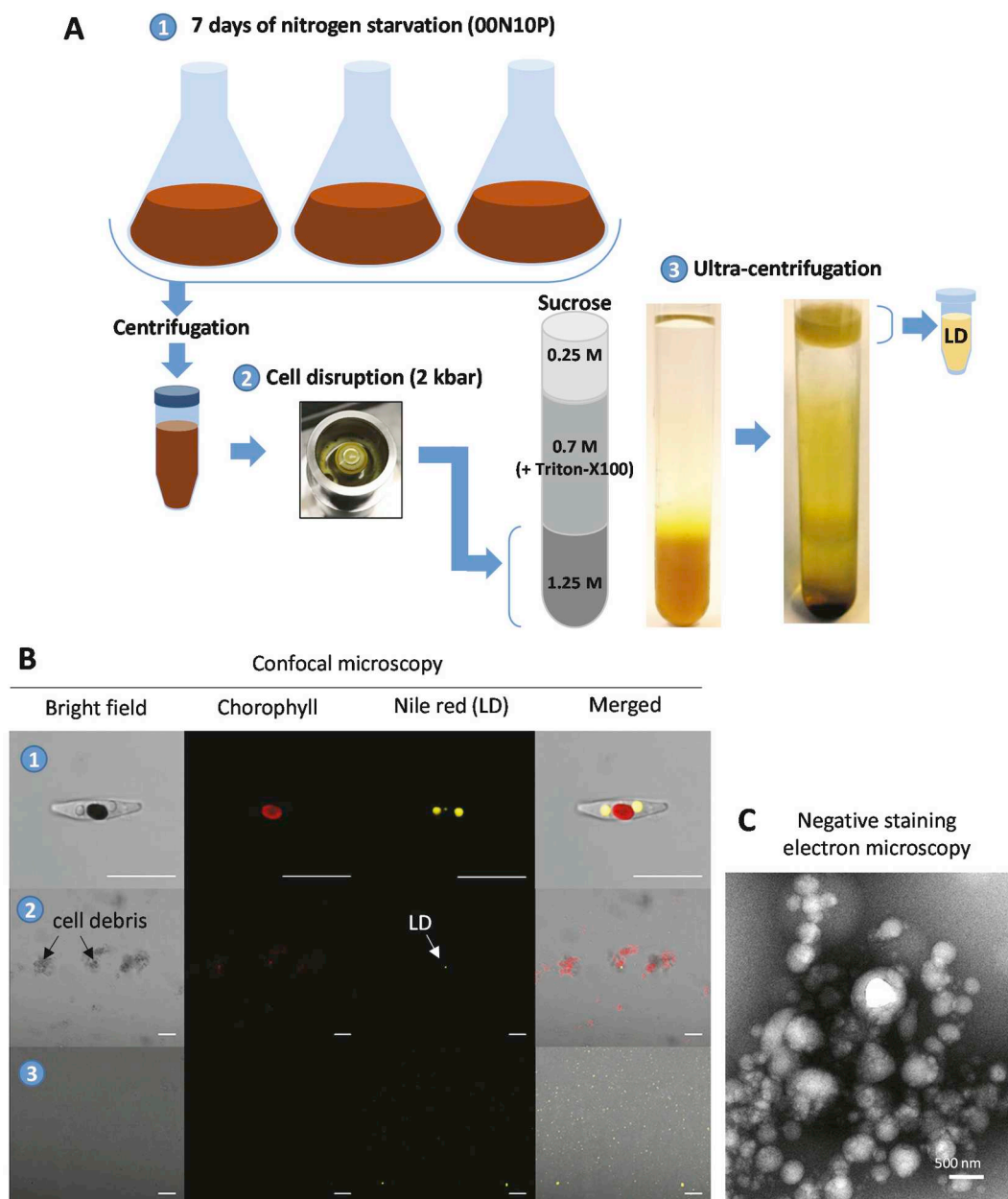


**Fig. 2.** LD purification from nitrogen-starved *P. tricornutum* cells. **A.** Main steps of the LD purification protocol. *P. tricornutum* cells starved for 7 days in a medium without nitrogen (ESAW 00N10P) (step 1). Cells were collected by centrifugation and broken by high pressure (step 2). The purification was carried out by adjusting the sucrose content of the broken cells to 1.25 M prior loading 4.5 mL at the bottom of a density gradient. A 7-mL layer containing 0.7 M sucrose and triton X-100 was added, so as to allow lower density organelles to be separated based on buoyancy, while weakly associated structures and proteins were washed away by the detergent. A 1.5-mL layer containing 0.25 M sucrose was then added at the top of the tube for LD complete purification. The tubes were centrifuged at 68,000  $\times$  g, 4 °C for 16 h and purified LDs were collected at the top of the gradients (step 3). **B.** Monitoring of LD enrichment by confocal imaging. Scale bars: 10  $\mu$ m. **C.** Purified LDs observed by negative staining electron microscopy. Scale bar: 500 nm. Purified LDs were analyzed from three independent biological replicates.

### 3.4. Specific enrichment of lipid droplets in $\beta$ -carotene

Purified LDs floating at the surface of the density gradient had a pale yellow color, whereas dense cell debris, at the bottom of the tube, were brown (Fig. 2A). We addressed the possible accumulation of pigmented carotenoids within LDs. Fucoxanthin is one of the main pigments in *P. tricornutum*, cultivated in either rich or nitrogen depleted condition [77]. In the present cultivation conditions in nitrogen rich (ESAW 10N10P) and nitrogen depleted (ESAW 00N10P) media, fucoxanthin represents > 40 mol% of total carotenoid and chlorophyll pigments (Fig. 4). In purified LDs, the same proportion of fucoxanthin was

measured (Fig. 4), suggesting that a nonspecific enrichment of this hydrophobic molecule might have occurred in the course of LD purification. However, whereas whole cells also contained high levels of diadinoxanthin, chlorophyllide *a* and chlorophylls *a* and *c*, only traces of these pigments could be detected in the LD enriched fraction, further supporting the high purity level of the obtained fraction. By contrast, LDs were strongly enriched in  $\beta$ -carotene representing 28.7 mol% of total LD pigments (Fig. 4). Since this carotenoid is extremely minor at the whole cell level, it appears as a specific component of the LD enriched fraction of *P. tricornutum*.



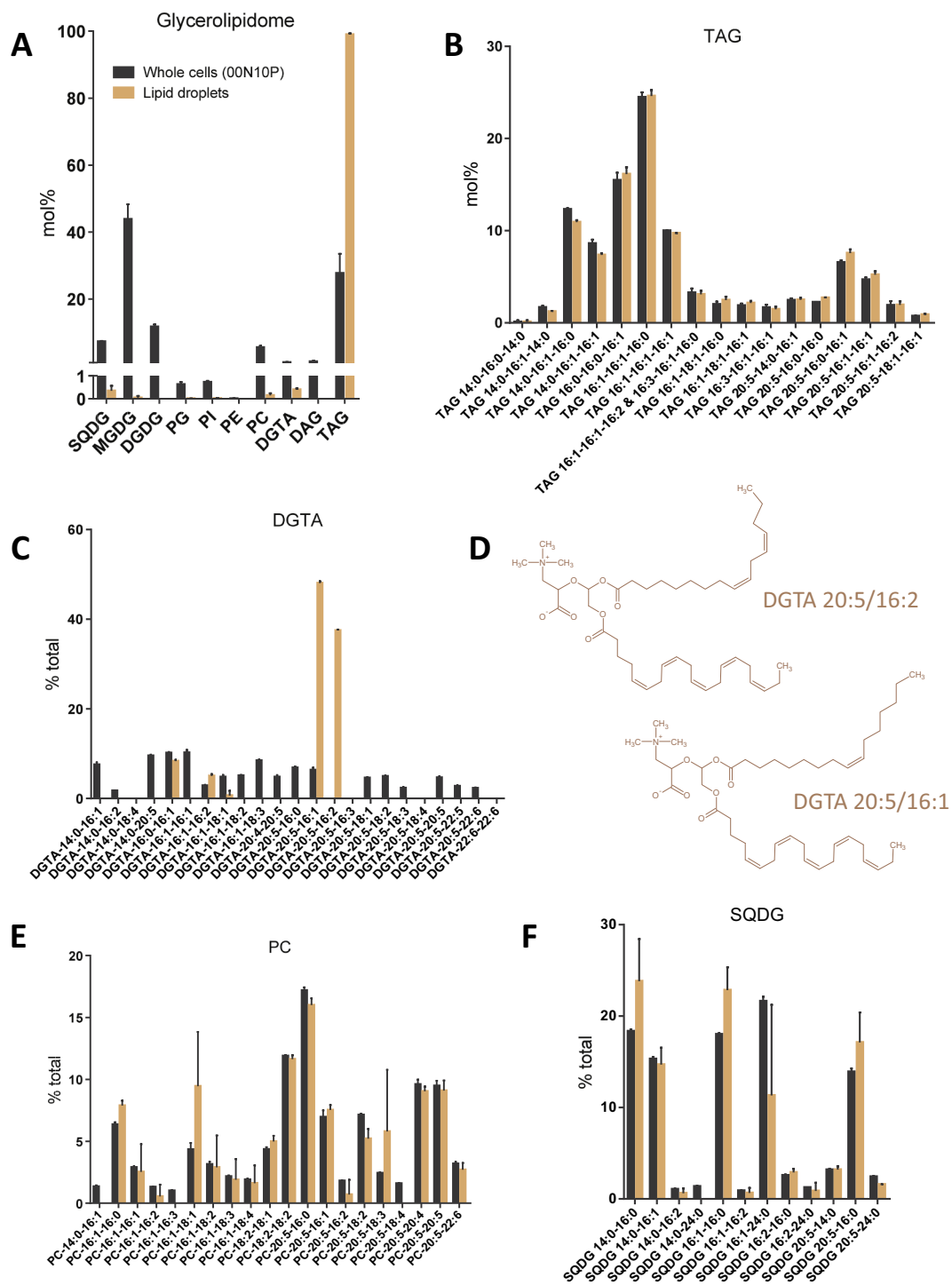


**Fig. 3.** Glycerolipids in *P. tricornutum* lipid droplets. Glycerolipids were extracted from whole cells cultivated in nitrogen starved medium (00N10P) and from lipid droplet (LD) purified fraction. A, Glycerolipid proportions in whole cells and purified LDs. B, TAG acyl profiles. C, DGTA acyl profiles. D, Chemical structures of the two major molecular species of DGTA in purified LDs. E, PC acyl profiles. F, SQDG acyl profiles. Glycerolipids and molecular species are expressed in mol%. Data correspond to biological triplicates ± standard deviation. DGDG, digalactosyldiacylglycerol; DGTA, 1,2-diacylglyceryl-3-O-2'-(hydroxymethyl)-(N,N,N-trimethyl)-β-alanine; MGDG, monogalactosyldiacylglycerol; PC, phosphatidylcholine; PE, phosphatidylethanolamine; PG, phosphatidylglycerol; PI, phosphatidylinositol; SQDG, sulfoquinovosyldiacylglycerol. Data obtained from whole cell extracts after cultivation in nitrogen depleted condition (00N10P) and from purified LDs are shown in black and orange, respectively.

**3.5. Analysis of the lipid droplet protein fractions using organelle-specific antibodies**

Cross contaminations and association of subcellular organelles with purified LDs are not easy to evaluate in *P. tricornutum* samples because specific antibodies are not readily available. We have therefore

developed a series of eight antibodies directed against protein markers of *P. tricornutum* cell compartments. Antigenic peptides were selected in the sequences of the Stramenopile Lipid Droplet Protein (StLDP, Phatr3\_J48859) [49], a SEIPIN known to act in the initial budding of nascent LDs (SEIPIN, Phatr3\_J47296) [78], a calnexin located at the ER (CNX, Phatr3\_J41172), the alpha subunit of the coatomer, known to act



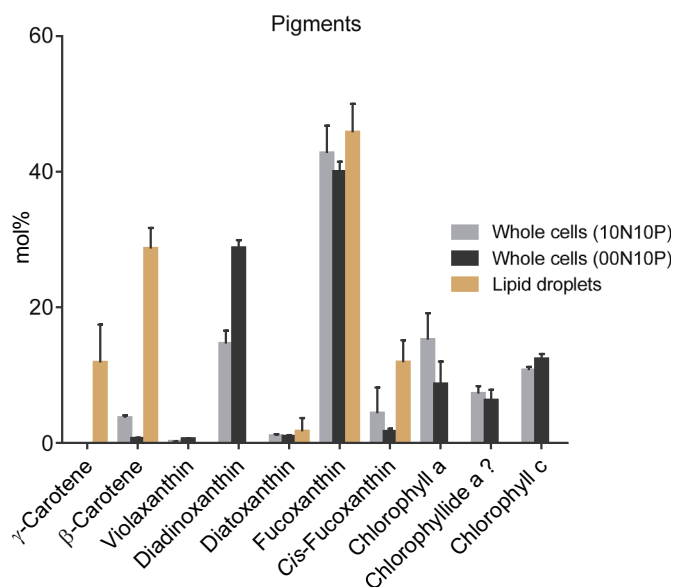


**Fig. 4.** Carotenoids in *P. tricornutum* lipid droplets. Carotenoids and chlorophylls from whole cells and purified LDs were extracted and analyzed as described in the Methods section. Pigments from whole cells cultivated in nutrient rich condition (10N10P), nitrogen starved condition (00N10P) and in purified LDs are shown in grey, black and orange, respectively. All pigments were determined by comparison with standard molecules. Error bars, standard deviation;  $n = 3$ .

in vesicular trafficking and to bind LDs in various systems [28] (COPA or COPI1, Phatr3\_J21929), the CGI-58 protein, located at the LD in mammals and at the peroxisome in plants [79–81] (CGI-58, Phatr3\_J54974), a peroxisomal biogenesis factor (PEX3, Phatr3\_J50623), an acyl-coA ligase 1 predicted to locate at the peroxisome (ACL1, Phatr3\_J17720), a mRNA export factor binding at the nuclear pores (RAE1, Phatr3\_J24439) and an isoform of triose phosphate transporter located at the outermost epiplastid membrane, EpM (see Fig. 1) [82] (TPT1, Phatr3\_J50742). We also used commercial antibodies raised against the gamma subunit of the coatomer, (Sec21p; Phatr3\_J10209), plastid proteins, i.e. the D1 subunit of photosystem II (PsbA; Q5D706), an iron-sulfur protein of photosystem I (PsaC; PsaC-phatc), and eventually the beta subunit of the mitochondria ATP-synthase (ATPβ chloroplastic and mitochondrial).

The yield in LDs following the procedure detailed here coupled with the protein extraction procedure used to eliminate TAG before SDS-PAGE, did not allow conventional protein quantification for the prepared samples; we therefore proceeded to an evaluation of the amount of proteins based on silver nitrate staining after SDS-PAGE separation (Fig. 5A). A known amount of *P. tricornutum* whole cell proteins (1.5 μg), obtained after cultivation in ESAW 10N10P or ESAW 00N10P media, was loaded in parallel with 2 μL of concentrated LD proteins, allowing to estimate a concentration of ~33 ng of LD proteins per μL. For Western blot analyses, we used 15 μg of whole cell proteins in parallel with 2 μg of concentrated LD proteins (Fig. 5B). We observed an increase in StLDP abundance in whole cell extracts when cells were grown in nitrogen starvation and we detected StLDP in the purified LD fraction (Fig. 5B). The antibody raised against the SEIPIN protein, acting early in the biogenesis of the LD, did not react with the purified LD fraction, suggesting that this protein was not associated with the mature LDs. For all other immunodetections, only CNX known to locate at the ER did react with the proteins extracted from purified LDs. Antibodies targeting the plastid envelope membrane, plastid thylakoids, peroxisome, mitochondria and the nuclear envelope did not react with the proteins extracted from purified LDs (Fig. 5B). In the specific case of RAE1, the protein was detected in whole cells grown in nutrient replete condition, but not upon nitrogen starvation, so the absence of reaction

of the anti-RAE1 antibody with LD proteins might simply reflect the absence of the antigenic protein. Altogether, these analyses support a high level of purity of obtained LDs. The purification procedure including the floatation through a gradient containing Triton-X100 has therefore washed the surface of LDs of possible contaminants. A loss of components bridging the LD to other organelles, such as the ER, the EpM, the mitochondria and/or the peroxisome cannot be excluded.

### 3.6. Mass spectrometry-based characterization and bioinformatic analysis of the lipid droplet proteome

Proteomic analyses of LD enriched fractions were performed using three independent biological replicates (samples named LD1, LD2 and LD3). For this, proteins were in-gel digested using trypsin before analysis of the resulting peptides using nano-LC-MS/MS. Obtained spectra were identified through searches against a compilation of sequences of the *P. tricornutum* protein database from the Ensembl Protists portal (12,178 entries) and the organellar-encoded proteins (165 entries). This strategy allowed to identify 326 different proteins in total (Supplemental Table S1). In order to build up a reference proteome of LDs from *P. tricornutum*, we set up stringency filters. We first decided to only take into account proteins highly confidently identified with a minimum of 3 peptides, selecting a sublist of 92 proteins (Fig. 6).

In order to select proteins associated with the LD specifically induced by nitrogen starvation, we applied a second filter based on proteins accumulating in whole cell extracts following a depletion of nitrogen. For this, we took advantage of results from another quantitative proteomic analysis of *P. tricornutum* whole cells, cultivated in rich (ESAW 10N10P) and nitrogen depleted (ESAW 00N10P) conditions (data not shown). We discarded from the list of LDs proteins six proteins found to be downregulated in the total proteome of nitrogen-depleted cells (Phatr3\_EG01907, Phatr3\_J55209, Phatr3\_draftJ1806, Phatr3\_J54477, Phatr3\_J49151 and gi|118411023|ref|YP\_874418.1| corresponding to the RUBISCO large subunit).

The LD proteome of *P. tricornutum* is presented in Table 1. First of all, we identified three of the five major proteins identified in the first proteomic study performed on *P. tricornutum* LD [49]: the Stramenopile Lipid Droplet Protein (StLDP, Phatr3\_J48859) that was confirmed to localize at its surface [51], the Lipid droplet acyl CoA binding protein (LD-ACBD, Phatr3\_J48778) and a Heat shock protein (HSP70A, Phatr3\_J54019).

The proteome revealed the presence of proteins belonging to the PAP (Plastid lipid associated protein)/Fibrillin family. This family of proteins is found on the surface of plastoglobules [83,84], a category of lipid bodies generated inside chloroplasts [85]. The generation of TAG-rich lipid droplets inside chloroplasts has been proposed [86], but was recently shown as very unlikely [87]. The detection of these proteins suggests therefore that a minor fraction of plastoglobules were recovered during the purification of cytosolic LDs.

Interestingly, none of the enzymes involved in TAG assembly, such as DGAT or PDAT, or in early biogenesis of the LD, such as SEIPIN, were present in the mature LD proteome. We did neither detect enzymes involved in massive hydrolysis of TAG, such as lipases, or CGI-58 known to be involved in lipogenesis in mammals and plants. The proteomic profile we obtained reflected therefore a rather stable and mature organelle. We classified the functional annotations of the 86 proteins in seven large groups: metabolism (19 proteins), membrane organelles (9 proteins), chaperones, protein folding, posttranslational modifications, quality control (12 proteins), cytoskeleton (3 proteins), genetic information processing (15 proteins), plastoglobules and thylakoid components (18 proteins) and unknown proteins (10 proteins) (Table 1).

Metabolic enzymes enriched in the LD purified fraction involved mainly cytosolic enzymes of the glycolytic and pentose phosphate pathways, and mitochondrial components of the Krebs cycle (Table 1). The plastid carbonic anhydrase (Phatr3\_J22357) and acetyl-CoA

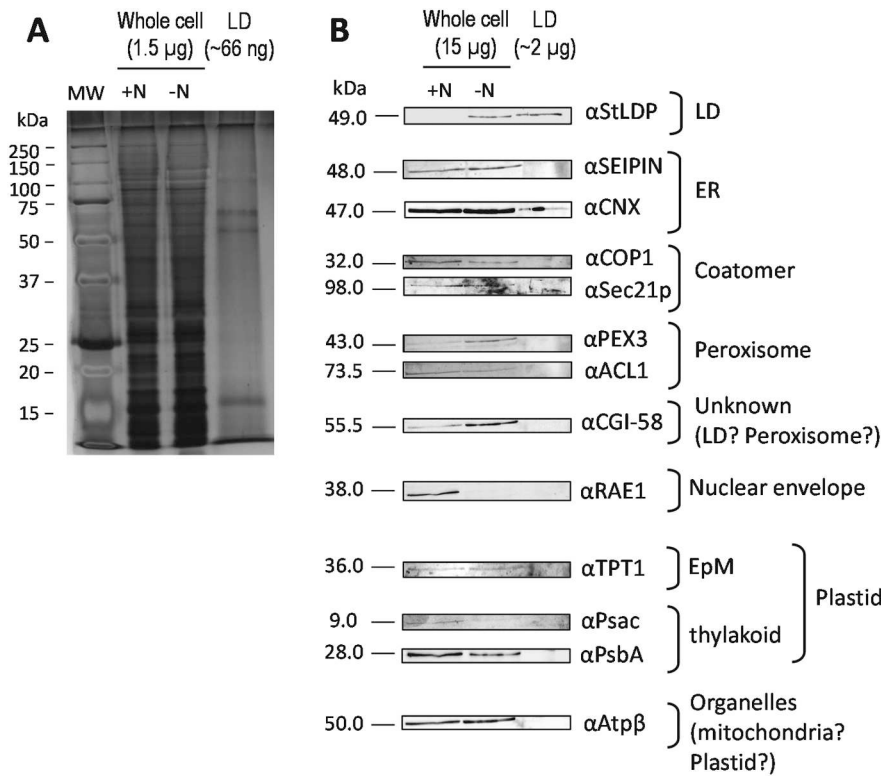


**Fig. 5.** Western blot analysis of the LD purified fraction. A, Silver nitrate staining of whole cell and lipid droplet protein extracts. A known amount of *P. tricornutum* whole cell proteins (1.5 µg), obtained after cultivation in ESAW 10N10P (+N) or ESAW 00N10P (-N) media, was loaded in parallel with 2 µL of concentrated LD proteins. The amount of protein in the purified fraction of LDs was evaluated by comparison at ~33 ng·µL<sup>-1</sup>. MW, Molecular Weight. B, Western-blot analysis of LD protein fraction using antibodies raised against membrane compartment markers. The purity of the LD purification was checked by using antibodies raised against different cell compartment markers: StLDP (LD), Seipin (ER), CNX (ER), COP1 and Sec21p (coatomer), PEX3 and ACL1 (Peroxisome), CGI-58 (unknown localization in *P. tricornutum*), RAE1 (Nuclear envelope), TPT1 (Plastid - EpM), PsbA (Plastid - thylakoid) and ATPβ (mitochondria and plastid). All antibodies were used at a dilution of 1/1000 except anti-CN X (αCNX) at 1/5000 and anti-ATPβ (αATPβ) at 1/2000.

carboxylase (Phatr3\_EG019955) indicate proximity of LDs with the initiation of fatty acid biosynthesis. Enzymes involved in the catabolism of amino acids, reallocating carbon toward lipids, were detected, i.e. a glutamine synthase (GS, Phatr3\_J22357), glutamate dehydrogenase (GDH, Phatr3\_J13951); agmatinase (AGMAT, Phatr3\_J40880) and urease (UREC, Phatr3\_J29702). Two important proteins involved in acyl-CoA metabolism were also found associated to LDs, i.e. a long chain acyl-CoA synthetase (ACS4, Phatr3\_J45510) and the LD-ACBD. The presence of plastid- and mitochondria-located enzymes suggests the presence of contact sites with these organelles.

LD contact with other organelles is supported by the detection of membrane proteins, mainly from endomembranes, such as two subunits of the COP1 coatomer (COPA; Phatr3\_J21929; COPBETA2, Phatr3\_J27518), two components of the clathrin vesicle coating system (CHC, Phatr3\_EG01984; PTAP1/2BETA, Phatr3\_draftJ1735), a V-ATPase (VATPase, Phatr3\_J51058) and a subunit of an ABC transporter (Phatr3\_EG02323). Contact with mitochondrial envelope is supported by the detection of an adenine nucleotide translocator at the inner mitochondrial envelope membrane (SLC25A4, Phatr3\_J22873).

Membrane proteins from the plastid, more precisely the EpM, were not identified, but it is not excluded that some of the unknown proteins listed here might be located at the EpM. Consistently with this hypothetical localization, 5 of the unknown proteins exhibit a putative signal peptide (Phatr3\_J44488, Phatr3\_J50215, Phatr3\_J49286, Phatr3\_J50214, Phatr3\_EG02301) based on the SignalP predictive method [63], one containing 3 transmembrane domains (Phatr3\_EG02301). One of the unknown proteins is predicted to contain a chloroplast transit peptide (Phatr3\_J55010) based on the ChloroP predictive method [64] and on the detection of an ASAFAP-motif specific to sequence import into secondary plastids [65].

LD fraction was enriched in chaperones and components of ubiquitin-regulated machineries controlling protein folding (Table 1). The translation of mRNA into proteins at the periphery of LDs appears therefore facilitated, and is further supported by the presence of 40S and 60S ribosomal subunits and three components of RNA translation machinery, i.e. Elongation factors 1-alpha and 2 (EF1A, Phatr3\_J28737; EF2, Phatr3\_J35766) and the Eukaryotic translation initiation factor 4A (EIF4A, Phatr3\_J25743). Ribosomes are often considered as non-

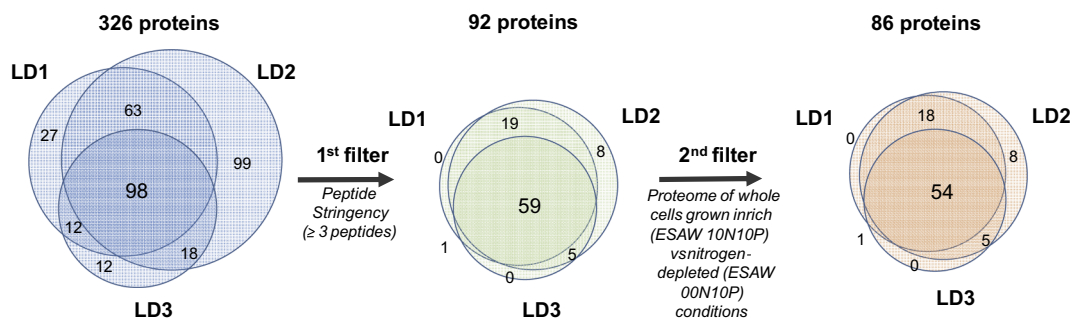


**Fig. 6.** Characterization of *P. tricornutum* LD core proteome. Proteomic analysis led to the identification of 326 proteins from three independent biological replicates of LD fractions from *P. tricornutum*. To build a reference LD proteome, 2 different filters were then applied. The first one led to the conservation of proteins identified with at least three tryptic peptides. The second filter corresponds to a subtraction of proteins detected in whole cells downregulated in nitrogen-starved condition (ESAW 0N10P) compared to nitrogen-rich condition (ESAW 10N10P). Six proteins were removed from the proteome of purified LDs.

**Table 1**  
 Proteome of the purified LD from *Phaeodactylum tricornutum*. Protein IDs were obtained from the Ensembl database, and when available, Uniprot accessions were provided. Number of trypsin peptides, sequence coverage, sequence length and the number of predicted transmembrane domains (TM) are indicated. (\*) localization based on [147].

Functional classification	Protein ID	Gene symbol	Description	Num. of pept	Seq. cover.	MW (kDa)	Seq. length	Score	Uniprot accession	Num. of TM	Localization
Fatty acids synthesis	Phatr3_EG01955	ACC1	Acetyl-CoA carboxylase 1	8	4.3	228.8	2082	68.877	B7G7S4	0	Plastid
	Phatr3_J45510	ACS4	Long chain acyl-CoA synthetase 4	8	14.7	73.186	667	76.902	B7FXX6	0	Cytosol
	Phatr3_J48778	LD-ACBD	Lipid droplet acyl CoA binding protein (Yoneda et al., 2016)	3	13.7	38.326	351	72.793	B7G8C2	4	Cytosol/lipid droplet
Glycolysis	Phatr3_J51128	GAPC2A	Glyceraldehyde-3-phosphate dehydrogenase	4	14.4	35.418	334	323.31	B7G6K6	0	Cytosol
	Phatr3_J22122	GAPC1	Glyceraldehyde-3-phosphate dehydrogenase	7	24.3	40.182	379	50.257	B7G5Q1	0	Cytosol
Pentose phosphate pathway	Phatr3_J14792	PGK	Phosphoglycerate kinase	4	12.2	45.979	436	33.992	B7G6H0	0	Cytosol
	Phatr3_EG02298	PGD	6-phosphogluconate dehydrogenase	3	2.3	125.38	1119	18.835	B7FUU0	0	Cytosol
	Phatr3_J41856	TKL	Transketolase	4	5.2	77.135	711	48.093	B7GSR3	0	Cytosol
	Phatr3_J29260	TKL	Transketolase	3	4.8	74.096	684	26.285	B7GSR3	0	Cytosol
Oxaloacetate biosynthesis	Phatr3_J27976	PTPEPC2	phosphoenolpyruvate carboxylase	6	6.6	111.88	1009	40.083	B7G1G6	0	Mitochondria*
	Phatr3_J30519	PYCI	Precursor of pyruvate carboxylase	3	3.3	136.07	1252	24.278	B7GBG1	0	Mitochondria
Krebs Cycle	Phatr3_J26921	SCSBETA	Beta chain succinyl-coa synthetase	3	8.6	47.621	443	22.113	B7FXA2	0	Mitochondria
	Phatr3_J26290	ACO2	Aconitase hydratase 2	3	3.4	106.67	989	31.174	B7FUR4	0	Mitochondria
	Phatr3_J51305	CA	Carbamic anhydrase	9	34.4	31.064	282	323.31	B7FNU0	0	Plastid
CO <sub>2</sub> concentration	Phatr3_J1305	CA	Carbamic anhydrase	9	34.4	31.064	282	323.31	B7FNU0	0	Plastid
	Phatr3_J22357	GS	Glutamine synthase	7	11.3	79.635	716	58.012	B7G6Q6	0	Cytosol
Glutamate catabolism	Phatr3_J13951	GDH	Glutamate dehydrogenase	3	8.2	49.458	450	19.966	B7G3X3	0	Cytosol
	Phatr3_J40880	AGMAT	Agmatinase	3	7.5	45.336	416	19.901	B7GCN5	0	Mitochondria
Ornithine-Urea cycle	Phatr3_J29702	UREC	Urease	3	4	94.032	878	19.026	B7G7W5	0	Cytosol
	Phatr3_J20885	GST	Glutathione S-transferase	3	11.7	34.621	307	18.389	B7G1M7	0	Mitochondria
Oxydoreduction	Phatr3_J48859	SLDP	Stramenopile Lipid droplet protein (Yoneda et al., 2016)	4	12.3	48.904	456	35.866	B7G8M1	2	Lipid droplet
	Phatr3_J13662	TM9SF	Nonaspanin	3	5.4	71.73	626	66.771	B7G2V6	9	Golgi/endosome
Unknown function, ER and plasma membrane	Phatr3_J21929	COPI/COPA	Coatomer subunit alpha	6	6	137.77	1254	89.602	B7G4Z7	0	TGN, ER, Lipid droplet?
	Phatr3_J27518	COPI/COP2	Coatomer, WD associated region	3	4.9	105.92	962	28.833	B7FZS9	0	TGN, ER, Lipid droplet?
Clathrin vesicle Formation	Phatr3_EG01984	CHC	Clathrin heavy chain	8	6.2	188.26	1672	121.18	B7G4Y3	0	Endocytic vesicles
	Phatr3_draftJ1735	PTAP1/2BETA	Beta subunit of clathrin adaptor complex AP2	5	6.7	98.631	890	58.116	B7S4C6	0	Plasma membrane
V-ATPase	Phatr3_J51058	VATPase	V-type H-ATPase subunit	3	13.7	27.891	255	29.119	B7G360	0	Endosome
	Phatr3_EG02323	ABC	ABC-transporter like protein, partial	7	4.3	253.01	2256	110.97	B7G0T6	1	Plasma membrane
Inner mitochondrial envelope membrane	Phatr3_J22873	SLC25A4	Adenine nucleotide translocator, ATP/ADP translocase	4	13.5	32.703	303	36.031	B7G8Y4	2	Mitochondria
	Phatr3_J46448	HSP	Heat shock protein, partial	5	20.3	31.711	281	323.31	B7G195	0	Cytosol?
HSP proteins - stress response	Phatr3_J54019	HSP70A	Heat shock protein HSP70 (Yoneda et al., 2016)	12	23.1	70.961	653	304	B7FQ84	0	Cytosol
	Phatr3_J55230	HSP90	Heat shock protein 90	7	11.8	80.548	709	97.087	B7GES3	0	Cytosol
Mitochondria-targeted chaperonin	Phatr3_J15138	HSP40	Heat shock protein 40/DnaJ heat shock protein (cochaperone of HSP70)	4	8	63.687	590	56.924	B7G7Z2	2	Cytosol
	Phatr3_J24820	CPN60	Chaperonin 60	3	6.6	62.509	594	25.989	B7FQ72	0	Mitochondria
Protein phosphorylation	Phatr3_EG02389	EPK2	EPK 2, cAMP-dependent protein kinase, partial	5	9.4	89.85	819	221.61	B7FUNI	0	Cytosol
	Phatr3_J45679	STK	Serine/threonine-protein kinase	3	6.2	75.453	713	54.773	B7FYI1	1	ER
Ubiquitination	Phatr3_J27118	UBI3	Ubiquitin extension protein 3	3	26.5	17.808	155	24.62	B7FY02	0	Cytosol/nucleus?
	Phatr3_J46098	PUR39	U-box domain-containing protein 39	4	9.4	66.442	618	53.625	B7G022	0	Unknown
Ubiquitin-dependent degradation by the proteasome	Phatr3_J1884	LAP	Leucyl aminopeptidase	5	11.1	66.881	629	48.741	B7FVX9	0	Cytosol

(continued on next page)

Table 1 (continued)

Functional classification	Protein ID	Gene symbol	Description	Numb. of pept	Seq. cover.	MW (kDa)	Seq. length	Score	Uniprot accession	Numb. of TM	Localization
ER associated protein degradation (ERAD)	Phatr3_J54642	HCDC48	AAA-type ATPase Cdc48	3	5.1	88.486	800	33.986	B5Y3R0	0	Plastid
	Phatr3_EG02643	BIP	ER luminal binding protein	6	10.5	72.265	659	46.858	B7FUB7	0	Endoplasmic reticulum
Cytoskeleton	Phatr3_J51157	ACT1	Actin/actin like protein	4	10.9	41.79	377	104.05	B7G878	0	Cytoskeleton
	Phatr3_J21122	TUBB	Tubulin beta	6	16.6	49.581	447	85.959	B5Y3W7	0	Cytoskeleton
40S small ribosomal subunit	Phatr3_J54534	TUBB	Tubulin beta	4	10.9	49.747	451	47.266	B7G0C3	0	Cytoskeleton
	Phatr3_J6847	RPS9	Ribosomal protein 9	3	18.8	21.272	186	100.7	B7FXJ2	0	Cytosol
	Phatr3_J30486	RPS18	Ribosomal protein 18 40S small ribosomal subunit	5	32.6	16.488	141	155.06	B7GB86	0	Cytosol
	Phatr3_J51066	RPS19	Ribosomal protein 19 40S small ribosomal subunit	3	12.5	17.09	152	22.599	B7G3G6	0	Cytosol
60S large ribosomal subunit	Phatr3_J17545	RPS3a	40S ribosomal protein S3a	5	19.9	28.921	261	44.111	B7FPM3	0	Cytosol
	Phatr3_draft1977	RPL4e	Ribosomal protein 4e 60S large ribosomal subunit	4	14.9	41.571	382	125.56	B7S3I7	0	Cytosol
Eukaryotic translation factor	Phatr3_J30315	RPL18	RPL18, ribosomal protein 18, 60S large ribosomal subunit	3	17.2	21.373	192	26.036	B7GAG0	0	Cytosol
	Phatr3_J30660	p0	60S acidic ribosomal protein p0	4	20.1	29.85	273	45.399	B7GBL1	0	Cytosol
	Phatr3_J28737	EF1A	Elongation factor 1-alpha	4	7.1	48.055	439	76.325	B7G3C4	0	Cytosolic/nuclear
	Phatr3_J35766	EF2	Elongation factor 2	5	6.4	82.337	749	51.095	B7FZ72	0	Cytosolic/nuclear
	Phatr3_J25743	EIF4A	Eukaryotic translation initiation factor 4A	3	8.2	47.206	414	20.355	B5Y531	0	Cytosolic/nuclear
	Phatr3_J54686	Era	GTPase Era	6	5.3	136.53	1226	38.352	B7G2A6	1	Mitochondria
	Phatr3_J34971	H4-1B	Histone H4	5	32	11.383	103	71.208	B7FX68	0	Cytosolic/nuclear
	Phatr3_J21239	H3.3	Histone H3	4	22.8	15.327	136	95.474	B7G218	0	Cytosolic/nuclear
	Phatr3_J54360	H2B-1B	Histone H2B	3	31.9	12.629	116	115.92	B7FWR8	0	Cytosolic/nuclear
	Phatr3_J50872	H3-1C	Histone H3	4	25	15.312	136	13.494	B7FR39	0	Cytosolic/nuclear
PAP fibrillin	Phatr3_J45813	PAPFIB	Plastid lipid-associated protein/fibrillin conserved domain protein	4	15.6	33.606	314	48.681	B7FYR9	0	Plastid
	Phatr3_J49943	PAPFIB	Plastid lipid-associated protein/fibrillin conserved domain protein	7	18.6	47.47	431	101.04	B7GCE0	0	Plastid
Pigments	Phatr3_J50705	LHCF4	Fucoxanthin-chlorophyll a-c binding protein C, chloroplastic	5	31.3	96.452	198	21.328	Q08586	0	Plastid
	Phatr3_J22006	LHCF10	Fucoxanthin chlorophyll a/c protein, chloroplastic	3	11.2	5.8	206	22.154	B7GSB6	0	Plastid
Photosynthesis	Phatr3_J51230	LHCF11	Fucoxanthin-chlorophyll a-c binding protein F, chloroplastic	4	17.8	24.085	197	21.275	Q41094	0	Plastid
	Phatr3_J22395	LHCF8	Fucoxanthin chlorophyll a/c protein	3	13.5	11.644	200	21.651	B7G6Y1	0	Plastid
	Phatr3_J15806	PDS-LIKE3	Phytoene desaturase-like protein	3	5.6	18.915	621	68.012	B7GA36	1	Plastid
	gi 118410963 ref YP_874358.1	psaB	Photosystem I P700 apoprotein A2	7	10.6	79.342	733	81.846	A0T0M7	10	Plastid
	gi 118410982 ref YP_874377.1	psbD	Photosystem II reaction center protein D2	3	9.4	78.031	351	39.077	A0T097	6	Plastid
	gi 19373561.3 ref YP_874376.2	psbC	Photosystem II chlorophyll A core antenna apoprotein CP43	3	8.7	43.852	459	50.141	A0T096	6	Plastid
ATP-synthase	Phatr3_J4937	ATP1	Rubisco expression protein	5	13.1	65.725	594	65.788	B7FR98	0	Plastid
	Phatr3_J42434	ATP1	Rubisco expression protein	4	14	56.116	484	52.383	B7FR99	0	Plastid
	Phatr3_J14618	ATP1	ATP synthase subunit alpha	12	26.1	58.048	544	159.28	B7G531	0	Plastid/ mitochondria?
ATP-synthase	Phatr3_J54086	ATPB	ATP synthase subunit beta	5	15	53.618	501	119.04	B7FS46	0	Plastid
	Phatr3_J20657	ATPC	ATP synthase gamma chain	7	26.9	42.297	390	71.62	Q41075	0	Plastid
	Phatr3_J24978	ATPCF1	ATP synthase CF1 alpha subunit	4	11.1	55.922	506	107.56	B7FQ08	0	Plastid
	gi 118411012 ref YP_8744407.1	atpB	ATP synthase CF1 beta chain	4	12	51.62	475	27.984	A0T0D2	0	Plastid
	gi 118411031 ref YP_874426.1	atpA	ATP synthase CF1 alpha chain	5	8.7	54.621	505	6.7554	A0T0F1	0	Plastid

(continued on next page)



Table 1 (continued)

Functional classification	Protein ID	Gene symbol	Description	Numb. of pept	Seq. cover.	MW (kDa)	Seq. length	Score	Uniprot accession	Numb. of TM	Localization
Predicted protein	Phatr3_J44488		Predicted protein	4	6.4	55.136	530	321.14	B7FUA4	0	Signal peptide
	Phatr3_J50215		Predicted protein	6	22.6	37.645	350	134.41	B7FXS8	0	Signal peptide
	Phatr3_J49286		Predicted protein	5	19.9	31.929	301	112.6	B7GA37	0	Signal peptide
	Phatr3_EG00979		Predicted protein, partial	3	14.2	30.696	289	26.467		0	?
	Phatr3_J55010		Predicted protein	3	3.1	92.085	843	40.202	B7G9R3	0	Plastid?
	Phatr3_J50214		Predicted protein	5	19	38.707	358	20.143	B7FXS9	0	Signal peptide
	Phatr3_J50236		Predicted protein	4	17	27.078	264	30.499	B7GDE6	0	?
	Phatr3_J13587		Predicted protein, partial	4	7.9	61.195	572	28.494		0	?
	Phatr3_J49287		Predicted protein	4	4.7	127.71	1174	23.128	B7GA38	0	Mitochondria
	Phatr3_EG02301		Predicted protein	6	5.8	131.31	1217	43.511	B7G3N9	3	Signal peptide

specific contaminants, but the detection of the complete flow from protein synthesis to folding and quality control appears as significant.

Eventually, the LD fraction was also enriched in four histone isoforms (H2B-1B, Phatr3\_J54360; H3-1C, Phatr3\_J50872; H3.3, Phatr3\_J21239; H4-1B, Phatr3\_J34971), a feature previously described in LDs from *Drosophila* embryos [88]. Histone association to LDs poses the question of a possible role of this organelle in the storage of some specific proteins, mainly histones, in a context where most proteins are degraded.

#### 4. Discussion

##### 4.1. Purity of the *P. tricornutum* LD fraction

A protocol for *P. tricornutum* LD purification has been described previously, by loading broken cells on top of a discontinuous gradient, followed by an ultracentrifugation so as to pellet higher density cell components [49]. We adjusted this first protocol to reduce contamination to a minimum. A possible alternative is to load broken cells at the bottom of the centrifugation tube, under a discontinuous gradient [70,71,89]. We therefore adjusted the broken cell suspension to 1.25 M sucrose and loaded this sample under a 0.7 M-sucrose layer containing Triton X-100. The addition of detergent aimed at washing the low-density LDs from contaminants and large cell debris, while moving to the top of the tube based on their buoyancy. This process might possibly remove weakly bound LD components, which might be lost in our analysis. A 0.25 M-sucrose layer was added at the top for the recovery of LD, without detergent. After 16 h of ultracentrifugation at 68,000 ×g at 4 °C, LDs were clearly separated from cellular debris as assessed by confocal and electron microscopy (Fig. 2). With 99 mol% of TAG and a barely detected amount of MGDG (Fig. 3), the LD fraction presented a high purity. We could also immunodetect the Stramenopile LD protein (StLDP), the only known marker of *P. tricornutum* LD [49,51] in the LD enriched fraction, whereas none of the antibodies raised against other cell compartments could cross-react with LD protein extracts, with the notable exception of an anti-calnexin (αCNX) (Fig. 5). Based on the antibody specificity, a lack of immunodetection might indicate an absence of the antigenic protein or a very low proportion compared to the main pool of this protein in another location of the cell. It is apparently contradictory that the COP1/COPA coatomer subunit could not be immunodetected in the LD fraction, whereas it was detected in the proteomic analysis performed on the same sample. The sensitivity of proteomic approach proved to be higher than the antibody we have developed, and the portion of COP1/COPA associated to LDs is likely much lower than that in other organelles, such as in the set of trafficking vesicles.

We observed a pale yellow color of the purified LD fraction, suggesting the presence of specific pigments. No significant difference was observed for fucoxanthin between total extracts and purified LD fraction (Fig. 4). However, chlorophylls a and c, which are parts of fucoxanthin-chlorophyll protein complexes (FCP) [90,91] were only detected in the total extracts and in very small proportion in the purified fraction. The fucoxanthin molecules we detected therefore belong to a distinct pool. The presence of other low-density lipid bodies from the stroma of the plastid is evidenced, since we detected marker proteins of plastoglobules, i.e. plastid lipid-associated protein (PAP) fibrillins (PAPFIB, Phatr3\_J45813 and Phatr3\_J49943) (Table 1). Plastoglobules are particular lipid bodies generated in the chloroplast, and could contain carotenoids. Their presence in the LD fraction cannot be avoided by a separation method based on density. They explain why some internal components of the plastid occur in the purified LD fraction, easily identified in the obtained proteome (about 20 proteins, out of 86, see below). The presence of plastoglobules, even in very minor amount, makes it difficult to assess whether the obtained carotenoid profile is strictly associated to the cytosolic LD or to these plastid lipid bodies. The unresolved localization of observed fucoxanthin also

applies to  $\beta$ -carotene, however the presence of this carotenoid in plastoglobules is unlikely and comparison with other eukaryotes supports its presence in cytosolic LDs in *P. tricornutum*.

#### 4.2. A hydrophobic core containing triacylglycerol and devoid of steryl esters

TAG making the bulk of *P. tricornutum* LD are localized in the hydrophobic core of the organelle. The composition of acyl molecular species in TAG did not differ from that in total extracts (Fig. 3) confirming that no undesired hydrolysis had occurred in the course of LD purification. We addressed the presence of other hydrophobic molecules, such as steryl esters, as reported in other eukaryote models [28–30], but we could not detect the presence of any such molecule. As discussed above, the hydrophobic core could also be enriched in fucoxanthin, at the end of synthesis of carotenoids and  $\beta$ -carotene (Fig. 4). The presence of pigments in cytosolic LDs has been described previously in the green alga *Haematococcus pluvialis*. In *H. pluvialis* astaxanthin (a red ketocarotenoid) is synthesized from  $\beta$ -carotene by the action of a  $\beta$ -carotene ketolase, when environmental conditions become unfavorable [92,93]. One model proposes an export of  $\beta$ -carotene from chloroplast to the ER, where it could be converted into astaxanthin, then astaxanthin ester and stored in LD [43,93–95]. In *P. tricornutum* a similar model might be proposed, based on an export of  $\beta$ -carotene from the plastid to the ER or the epiplastid membrane. A gene encoding a putative lycopene cyclase (Phatr3\_J8835) can be detected in the genome of *P. tricornutum*. However, the corresponding protein was not detected in the LD proteome, raising questions about its location and function.

#### 4.3. A limiting monolayer containing sulfoquinovosyldiacylglycerol, phosphatidylcholine, brassicasterol and specific molecular species of the betaine lipid

The glycerolipidome of *P. tricornutum* LD contains 0.4 mol% of DGTA, 0.35% of SQDG and 0.15% of PC. Based on the glycerolipid profile of whole cells, dominated by MGDG, the presence of only traces of this galactolipid highlights that detected polar lipids are not contaminants but actual components of the monolayer encapsulating LDs. The presence of SQDG, usually restricted to plastid membranes [5] is therefore remarkable and suggests that the membrane at the origin of the LD in *P. tricornutum* should contain this lipid. By contrast, PC [96] and betaine lipid [97] are usually synthesized in the ER. PC is a glycerophospholipid frequently found in the LD monolayer of several study models, such as mammals [98] or yeasts such as *Saccharomyces cerevisiae* [75,99] and *Pichia pastoris* [100]. PC is known to relocate to the outer leaflet of the outer envelope membrane in primary chloroplasts [101], so it is possible that part of PC lies in the outermost membrane of the plastid in *P. tricornutum*. Eventually, brassicasterol is detected in purified LDs. Sterols are usually restricted to endomembranes and absent from plastids. Nevertheless, they have been detected in the non-photosynthetic secondary plastid in the Apicomplexa *Plasmodium falciparum* [102], and similarly, brassicasterol could also be localized in *Phaeoactylum* plastid membranes.

The precise composition of the four membranes limiting diatom's plastid has not been determined to date [5]. The hybrid presence of a plastid lipid (SQDG) and ER lipids (DGTA, PC, brassicasterol) we report here, supports therefore that the membrane producing LDs is the outermost membrane of the plastid, the epiplastid membrane (EpM). A major question raised by our results is the origin of SQDG in the EpM, either following an export from a site of synthesis within the plastid, or the presence of a synthesis pathway in the EpM.

DGTA is a betaine lipid, a class of glycerolipids, which is not conserved in the evolution of eukaryotes, having two fatty acids esterified in the *sn*-1 and *sn*-2 position and a betaine group connected by an ether bond in the *sn*-3 position (Fig. 3). Three betaines lipid are described in the literature:

1,2-diacylglycerol-3-O-2'-(hydroxymethyl)-(N,N,N-trimethyl)- $\beta$ -alanine (DGTA), 1,2-diacylglycerol-3-O-4'-(N,N,N-trimethyl)-homoserine (DGTS) and 1,2-diacylglycerol-3-O-carboxy-(hydroxymethyl)-choline (DGCC). In phosphate deficiency, betaine lipids accumulate in many organisms including diatoms [14,103]. Phosphate starvation leads to a degradation of phospholipids, releasing phosphate for recycling purposes, and current models propose that betaine lipids could compensate the subsequent lack of phospholipids [104]. In systems like diatoms, and based on the present study, betaine lipids could also help in LD biogenesis.

Two molecular species of DGTA are strikingly enriched in *P. tricornutum* LD, with a very simple fatty acyl profile, i.e. containing eicosapentaenoic acid paired with palmitoleic or palmitolenic acids, DGTA 20:5/16:1 and DGTA 20:5/16:2 respectively. The betaine lipid is considered as a platform to synthesize C20:5 very-long chain polyunsaturated fatty acids (VLC-PUFAs), as evidenced by the presence of fatty acid precursors, i.e. C18:1, C18:2, C18:3 and C20:4 in DGTA [24,105–107]. The DGTA molecular species of LDs do not contain these precursors and are therefore sorted downstream C20:5 biosynthesis. Their synthesis should therefore occur in another subcellular location, likely in ER membranes disconnected from the EpM. Furthermore, in the lipidome of *P. tricornutum*, C16:2 is mainly present in MGDG and DGDG and seems absent from ER glycerolipids [14]. The detection of this fatty acid in this pool of DGTA supports an origin from the plastid.

The biosynthetic pathway of betaine lipids was reported only for DGTS in the *Chlamydomonas reinhardtii* and *Nannochloropsis oceanica* models [108,109], and involves a betaine lipid synthase (BTA1). A BTA1 homologue, called BTA1-Like (Phatr3\_J42872) has been identified in *P. tricornutum* [20,109]. In two recent transcriptomic studies of *P. tricornutum* exposed to stress leading to TAG accumulation, i.e. following exposure to nitric oxide [20] and to 17 $\alpha$ -ethynylestradiol, a derivative of the natural estrone and estradiol hormones [24], the gene encoding the BTA-like enzyme was upregulated. In the case of 17 $\alpha$ -ethynylestradiol treatment, the overexpression of the betaine lipid synthase coincided with the disruption of the very-long chain polyunsaturated fatty acid synthesis, marked by a decrease of eicosapentaenoic acid (20:5) and an increase in precursor fatty acids (C18:2, C18:3 and C18:4) [24]. We did not find any data regarding the level of expression of BTA1-Like in transcriptome datasets of *P. tricornutum* following nitrogen deficiency [110,111] and the expression of this gene should therefore be investigated in the future to assess whether its expression correlates with LD biogenesis in all known conditions.

Brassicasterol (24-methylcholest-5,22-dien-3 $\beta$ -ol) is the final product of the sterol biosynthesis pathway in *P. tricornutum* [73]. Sterols and TAG share a common starting point in their biosynthesis, acetyl-CoA, also used for the synthesis of fatty acids in the plastid. Sterols and TAG are therefore in competition with respect to carbon allocation. This was illustrated by either genetic or chemical impairment of sterol synthesis leading to an increase in TAG [24,73]. Based on the polarity of brassicasterol and on its proportion in LD (< 5 mol% brassicasterol, compared to sterol + glycerolipids), we suppose that this free sterol is at the periphery and in the polar lipid monolayer of the LD.

#### 4.4. A proteome indicating a proximity with the endomembrane system

Among the set of 86 proteins (Table 1), we detected six proteins involved in endomembrane trafficking. We first detect two coatomer proteins in the purified lipid LD fraction, COPA (Phatr3\_J21929) and COPBETA2 (Phatr3\_J27518). These two proteins are part of the COP1 complex. This complex is composed of seven subunits ( $\alpha$ ,  $\beta$ ,  $\beta'$ ,  $\gamma$ ,  $\epsilon$ ,  $\delta$ ,  $\zeta$ ) and participates in the retrograde transport of vesicles from *trans*-Golgi network to endoplasmic reticulum and in *intra*-Golgi transport [112]. In the unfiltered initial proteome (326 proteins), two other components of the coatomer were present (COPBETA, Phatr3\_J54511; and COPGAMMA, Phatr3\_J10209) (Supplemental Table S1). Based on the lack of immunodetection of COPA in the LD fraction using an anti-COP1

antibody reacting with proteins from whole cell extracts (Fig. 5), we deduce that only a small fraction of cell COP1 is associated with LD, whereas the rest is likely associated with retrograde vesicles. In *Drosophila*, the COP1 protein complex regulates the composition of perlipines on the surface of the LD and promotes the association of Adipose Triglyceride Lipase (ATGL) on the surface of the LD to initiate lipolysis [113]. Four subunits ( $\alpha$ ,  $\beta$ ,  $\gamma_1$  and  $\gamma_2$ ) of COP1 were also found in the LD proteome of mouse testicular Leydig cells [114]. The complex COP1 is dependent on the presence of ARF1 for its operation [115]. Using an in vitro system, the ARF1/COP1 machinery was shown to allow the synthesis of nano LDs of 60 to 80 nm in mammalian cells, acting therefore in LD homeostasis [116]. In this study, ARF1/COP1 proteins not only localize to LDs to bud nano-LDs, but they are required for targeting specific TAG-synthesis enzymes to LD surfaces. In the unfiltered set of 326 proteins identified in *P. tricornutum* purified LDs, we identified 5 small GTPases (ARF1, Phatr3\_J43251; RAB1A, Phatr3\_J22713; RABX1, Phatr3\_draftJ998; RAN1, Phatr3\_J51169 and Phatr3\_J36721), including ARF1, suggesting that a similar machinery might operate at the periphery of LDs, possibly controlling the budding of nano-LDs and/or addressing specific enzymes to its surface.

The proteome of *P. tricornutum* LD also highlights two proteins involved in the formation of clathrin, i.e. clathrin heavy chain (CHC, Phatr3\_EG01984) and the beta subunit of clathrin adaptor complex AP2 (Phatr3\_draftJ1735) (Table 1). The alpha subunit of clathrin adaptor complex AP2 (AP1 alpha, Phatr3\_J54442) was detected in the unfiltered proteome (Supplemental Table S1). Clathrins participate in protein transfer outside the *trans* Golgi network [117]. AP1 is involved in autophagosome formation from *trans* Golgi network [118]. The presence of these components further supports a connection with specific cytosolic vesicles. In the unfiltered proteome, we also identified 5 SNARE (Soluble N-ethylmaleimide-sensitive-factor Attachment protein REceptor) proteins (Supplemental Table S1). SNARE proteins are necessary for fusion of transport vesicles with target membranes [119]. These proteins are notably involved in the COP1 transport as well as in the autophagy mechanism. The SNARE proteins are divided into two categories: R-SNARE (formerly v-SNARE, v for vesicle) and Q-SNARE (formerly t-SNARE, t for target). Fusion between two membranes is favored by the formation of a four-helix bundle composed of one R-SNARE and three Q-SNARE [120]. R corresponds to the addition of an arginine during the fusion whereas Q corresponds to the addition of a glutamine. Of the five SNAREs detected, only one corresponds to a Q-SNARE (Syntaxin-61, Phatr3\_EG02404). The other four proteins are R-SNARE (VAMP72, VPS9D1, VPS41 and VPS). VPS proteins are involved in the docking of vesicles to their target membrane [119]. Three other proteins detected in the unfiltered LD proteome are also involved in mechanisms of autophagy and clathrin formation, two annexins (ANX, Phatr3\_J44109 and ANXA1, Phatr3\_J54190) completing the non-aspanin (TM9SF, Phatr3\_J13662) detected in the filtered set. A recent study of *P. tricornutum* proteome highlighted an increase in endocytosis and phagosomal activities in nitrogen depleted conditions [121]. The uncharacterized membrane compartment observed by electron microscopy in the vicinity of *P. tricornutum* LDs shows vesicles inside a membrane sack and could possibly correspond to an autophagosome, as observed in other cell types [122,123] (Fig. 1, indicated by a star). The role of these components at the periphery of LDs should therefore be addressed in future works.

We detected a Vacuolar-Type H<sup>+</sup>-ATPase (Phatr3\_J51058) in the filtered list and 6 additional V-ATPases in the unfiltered one (Phatr3\_J10862, Phatr3\_J27923, Phatr3\_J29711, Phatr3\_J15844, Phatr3\_J28794 and Phatr3\_J21030). V-ATPases correspond to a family of proton pumps using hydrolysis of ATP to produce a proton gradient in endomembrane vesicles and compartments. This kind of pump is usually found in secretory vesicles as well as in endosomes and lysosomes [124]. A V-ATPase was previously detected in the proteome of the alkenone body (a particular LD storing very long chain ketones) of *Tisochrysis lutea* [125]. Together with components of the endoplasmic-

reticulum-associated protein degradation (ERAD) pathway located in the ER (see below), the proteome of *P. tricornutum* LDs suggests tight connections with different compartments of the endomembrane system (ER, Golgi, Trans-Golgi, trafficking vesicles, clathrin-coated vesicles), consistently with contacts observed by electron microscopy (Fig. 1). The structure and function of these contact sites now need to be structurally and functionally characterized.

#### 4.5. A putative site for mRNA storage and a platform for specific synthesis and folding of proteins, coupled with the ERAD quality control system

The *P. tricornutum* LD proteome contains four proteins involved in post-translational modifications such as ubiquitination (UBI3 - Phatr3\_J27118 and PUB39 - Phatr3\_J46098) and phosphorylation (STK - Phatr3\_J45679 and EPK2 - Phatr3\_EG02389). Ubiquitination was previously shown to be a significant post-translational modification controlling lipolysis in plants [126]. Oleosins on the surface of the oleaginous seed LDs are thus ubiquitinated by the attachment of distinct ubiquitin motifs (monoubiquitin Ub, K48-linked diubiquitine K48Ub<sub>2</sub> and K63-linked diubiquitine K63Ub<sub>2</sub>) allowing addressing this protein to the 26S proteasome in the cytosol for its degradation [127]. It has been recently shown, by two independent teams, in the pollen tube of *Nicotiana tabacum* and in germinating seedlings of *Arabidopsis thaliana*, that the protein PUX10 (Plant UBX Domain-containing Protein 10), located on the surface of LDs, participated in the recognition of polyubiquitinated K48 motifs with its UBA domain [127,128]. PUX10, via its UBX domain, recruits the AAA-type ATPase Cell Division Cycle 48 protein (CDC48), a protein involved in the ERAD (Endoplasmic-reticulum-associated protein degradation) pathway. CDC48 is a protein that facilitates the transfer of polyubiquitinated misfolded protein to the 26S proteasome. Interestingly, the CDC48 (Phatr3\_J54642) protein is present in *P. tricornutum* LD proteome (Table 1). A second protein involved in the ERAD pathway has also been detected, an ER luminal binding protein (BIP - Phatr3\_EG02643), further supporting the association of this system of the LD. BIP participates in the recognition of misfolded proteins, in particular by recognizing hydrophobic regions exposed in an aqueous environment [129,130]. The LD proteome also contains PUB39, belonging to the family of U Box proteins. U box proteins are a family of E3 ubiquitin-protein ligases [131]. E3 ligase participates in the last reaction of the ubiquitination mechanism by recognizing misfolded substrates. Four 26S proteasome proteins (Phatr3\_draftJ706, Phatr3\_J45122, Phatr3\_EG00274, Phatr3\_J11735) were also detected in the unfiltered proteome, as well as a protein involved in the recognition of misfolded proteins, a C-type lectin domain family 4 member F (CLEC4F - Phatr3\_J50047) (Supplemental Table S1). Altogether, the presence of protein involved in ubiquitination processes and members of the ERAD pathway in the LD proteome suggests that control of the misfolded proteins is achieved at the periphery of this organelle.

Detection of misfolded proteins occurs downstream protein synthesis and folding. Consistently, chaperones, including four heat shock proteins (HSP, Phatr3\_J46448; HSP70A, Phatr3\_J54019; HSP90, Phatr3\_J55230, and HSP40, Phatr3\_J15138) were detected (Table 1). The translation of mRNA into proteins at the periphery of LDs is further supported by the presence of 40S and 60S ribosomal subunits and three components of RNA translation machinery, i.e. Elongation factors 1-alpha and 2 (EF1A, Phatr3\_J28737; EF2, Phatr3\_J35766) and the Eukaryotic translation initiation factor 4A (EIF4A, Phatr3\_J25743). Since aminoacids are nitrogen-rich molecules, protein synthesis is not expected in a nitrogen starved context [121,132,133], so the presence of this equipment could find a rational, either for the translation of a specific subset of mRNA, or in preparation of a massive production of proteins when the cells are not stressed any more. In line with this hypothesis, the RAE1 (Ribonucleic Acid Export 1) component of nuclear pore complex, involved in mRNA export [134], was not immunodetected in whole cell extracts after cultivation in the absence of



nitrogen (Fig. 5). We can therefore suppose that the recovery of cells relies on mRNAs stored in the cytosol during starvation. The vicinity of LDs might represent such a site for storing specific pools of mRNA.

#### 4.6. A site for histone protein storage?

Eventually, we detected four histones (H2B-1B, Phatr3\_J54360; H3-1C, Phatr3\_J50872; H3.3, Phatr3\_J21239 and H4-1B, Phatr3\_J34971) in the purified fraction of LDs. These histones are components of the octamer forming the nucleosomes. When also considering proteins with < 3 trypsin peptides (240 proteins, Supplemental Table S1), we could also detect other histones of the nucleosome (H2A-3A, Phatr3\_J34798; H2A-1, Phatr3\_J28445) as well as the H1 linker (H1, Phatr3\_J44318). Histones were detected in purified fractions of LDs from other organisms: *Drosophila melanogaster* young whole embryos [135], the tobacco sphinx *Manduca sexta* [136], the filamentous fungi *Mortierella alpina* [137], Mammalian cells like adipocyte [138], macrophages [139],  $\beta$ -pancreatic cells [140] and in adipose tissue [141].

In the case of *Drosophila melanogaster*, whereas present in embryo, these histones were not detected in the abdominal fatbody proteome [142]. The specific association of histones to embryo-LDs is ensured by the Jabba protein [88]. We did not identify any Jabba homologue in the genome of *P. tricornutum*, suggesting that another protein might recruit histones to the surface of LDs. The storage of these nucleosome components may prepare cell division and chromatin packaging, when cells are not stressed anymore.

#### 4.7. Can we learn from a proteome obtained with a lower stringency?

Proteomic analyses of the LD allowed the detection of 326 proteins in the purified fraction. We applied two filters to limit the detection of unspecific contaminants, one based on peptide stringency and one based on a decrease at whole cell level following nitrogen starvation. These filters have reduced the number of proteins to 86. Although it helped remove unspecific contaminants, as stated above, this procedure may also lead to a loss of information on the protein composition of LDs. We sought whether components commonly encountered in LD proteomes, had been identified in this initial list. Concerning LD biogenesis, Seipin is an ER protein having two transmembrane domains and a luminal loop, involved in LD early development [143]. A functional study of *P. tricornutum* Seipin (Phatr3\_J47296) suggests a similar role [78]. This protein is generally not detected in LD proteomes and we did not detect this sequence in the initial list, consistently with Western blot analyses (Fig. 5). Concerning TAG biosynthesis, we did not detect any enzymes responsible for the last step of synthesis, such as DGAT or PDAT, often detected in LDs. In the set of 86 proteins, three proteins were detected as participating in lipid metabolism: a fatty acid synthesis enzyme, Acetyl-CoA carboxylase 1 (ACC1, Phatr3\_EG01955) and two proteins involved in acyl-CoA homeostasis, a long chain acyl-CoA synthetase 4 (ACS4, Phatr3\_J45510), a class II protein, and a LD acyl-CoA binding protein (LD-ACBD, Phatr3\_J48778) previously described [49]. In the unfiltered set, we could detect 11 proteins involved in lipid metabolism, including fatty acid synthesis (triose phosphate/phosphate translocator, TPT1, Phatr3\_J24610; 3R-hydroxyacyl-ACP dehydrase, FABZ\_1, Phatr3\_J1143), acyl-CoA biosynthesis (long chain acyl-CoA synthetase, ACS1, Phatr3\_J20143) and  $\beta$ -oxidation in the mitochondrion (acyl-CoA deshydrogenase-like protein, ACAD, Phatr3\_J11014) (Supplemental Table S1). CGI-58 is one of the proteins frequently associated with LDs [79–81] (Phatr3\_J54974) and past studies in the diatom *Thalassiosira pseudonana* indicated a role of CGI-58 in LD hydrolysis [144]. CGI-58 was neither detected in the unfiltered LD proteome, nor by LD immunostaining with an anti-CGI-58 antibody (Fig. 5) Either CGI-58 is localized at the peroxisome level as in higher plants [145], or it might associate to LDs in conditions where TAGs need to be hydrolyzed. Eventually, the detection of TPT1 (Phatr3\_J24610) in the unfiltered proteome of *P. tricornutum* LD supports a tight association

with the surface of the outermost membrane of the plastid. We have developed an antibody against TPT1, with a moderate reactivity at the whole cell level (Fig. 5).

## 5. Conclusion

This work allowed the most refined characterization of the architecture of the LD in a diatom, upon nitrogen starvation. The LD of *P. tricornutum* has a hydrophobic core mainly composed of TAG. We also detected brassicasterol and  $\beta$ -carotene. The hydrophobic core is surrounded by a monolayer of polar lipids composed of DGTA (DGTA 20:5-16:1 and DGTA 20:5-16:2) and PC, possibly from the ER, and SQDG from the plastid. The extremely low content in MGDG does not support a biogenesis from the innermost two membranes (the IEM and OEM) of the plastid. Together with electron microscopy observation and the detection of TPT1 in the LD proteome, these results support a biogenesis of LDs from the outermost membrane of the plastid, the EpM. The origin of SQDG in the EpM, either by a transfer from more internal membranes or by in situ synthesis needs to be determined. Likewise, the export of a specific DGTA molecular species from other endomembranes to the EpM had never been shown or hypothesized prior to this work. This localization is consistent with the recent discovery of a TAG lipase associated to the chloroplast limiting membranes in *P. tricornutum* [146]. The LD proteome obtained in three independent biological replicates, based on detection of at least three trypsin peptides, and following subtraction of proteins downregulated by nitrogen starvation, highlights 86 proteins, including the only protein marker known for *P. tricornutum* LD (StLDP). Based on this most 'stringent' list, free of contaminants, we could identify connections with specific compartments and families of proteins, confirmed by the identification of additional components in the unfiltered complete LD proteome. LD-associated proteins suggest connections with vesicular trafficking (coatamer, clathrin), cytoskeleton, plastid and mitochondria. Unsuspected LD-associated functions include protein synthesis (ribosomes), folding (chaperones), posttranslational modifications and quality control (ubiquitination and ERAD pathway), possibly preparing translation of specific mRNAs. The detection of all histone proteins, as previously demonstrated in LDs from *drosophila* embryos, also suggests the storage of these nucleosome components, preparing cell division and chromatin packaging, when cells are not stressed anymore. Functional characterization and cellular localization studies should be conducted in the future to better understand the role of these proteins in *P. tricornutum*, in the course of LD formation and degradation, and in the context of nitrogen availability and other environmental stresses.

Supplementary data to this article can be found online at <https://doi.org/10.1016/j.algal.2019.101415>.

## Acknowledgements

This work was supported by a Flagship program from the CEA High Commissioner and the French National Research Agency (Oceanomics Project No. ANR-11-BTBR-0008, GlycoAlps Project No. ANR-15-IDEX-02 and ANR-10-INBS-08 ProFI).

## List of author contributions

J.L. performed most of the experiments. C.M. provided support for lipid droplet purification. A.J. provided support for confocal imaging. S.B., K.S., M.T. and Y.C realized the proteomic analyses. H.S. performed sterol analyses. M.K. performed pigments analyses. J.S. designed the antibodies for Western blotting analyses. D.F., P.H.J. and J.L.P. performed electron microscopy analyses. J.J. and F.R. provided specific expertise in glycerolipid analyses. E.M. conceived the project. All the authors contributed to the writing of the article.



## Conflict of interests

Authors declare that there is no financial or other interests that could be perceived to influence the outcomes of the research.

## Statement of informed consent, human/animal rights

No conflicts, informed consent, human or animal rights applicable.

## Author's agreement to authorship

All authors have seen, approved and are fully conversant with the contents of the manuscript, and agree to authorship and submission of the manuscript for peer review.

## References

- [1] D.A. Caron, P.D. Countway, A.C. Jones, D.Y. Kim, A. Schnetzer, Marine protistan diversity, *Annu. Rev. Mar. Sci.* 4 (2012) 467–493.
- [2] E. Marechal, Primary endosymbiosis: emergence of the primary chloroplast and the chromatophore, two independent events, *Methods Mol. Biol.* 1829 (2018) 3–16.
- [3] G.I. McFadden, Chloroplast origin and integration, *Plant Physiol.* 125 (2001) 50–53.
- [4] F.A. Wollman, An antimicrobial origin of transit peptides accounts for early endosymbiotic events, *Traffic* 17 (2016) 1322–1328.
- [5] D. Petroustos, S. Amiar, H. Abida, L.-J. Dolch, O. Bastien, F. Rébeillé, J. Jouhet, D. Falconet, M.A. Block, G.I. McFadden, C. Bowler, C. Botté, E. Maréchal, Evolution of galactoglycerolipid biosynthetic pathways – from cyanobacteria to primary plastids and from primary to secondary plastids, *Prog. Lipid Res.* 54 (2014) 68–85.
- [6] Z. Fussy, M. Obornik, Complex endosymbioses I: from primary to complex plastids, multiple independent events, *Methods Mol. Biol.* 1829 (2018) 17–35.
- [7] T. Cavalier-Smith, Kingdom chromista and its eight phyla: a new synthesis emphasising periplastid protein targeting, cytoskeletal and periplastid evolution, and ancient divergences, *Protoplasma* 255 (2018) 297–357.
- [8] A.S. Benoiton, F.M. Ibarbalz, L. Bittner, L. Guidi, O. Jahn, S. Dutkiewicz, C. Bowler, The evolution of diatoms and their biogeochemical functions, *Philos. Trans. R. Soc. Lond. Ser. B Biol. Sci.* 372 (2017).
- [9] O. Levitan, J. Dinamarca, G. Hochman, P.G. Falkowski, Diatoms: a fossil fuel of the future, *Trends Biotechnol.* 32 (2014) 117–124.
- [10] J. Lupette, Eric Maréchal, Phytoplankton Glycerolipids, Challenging but Promising Prospects from Biomedicine to Green Chemistry and Biofuels, Wiley VCH, Weinheim, Germany, 2018.
- [11] M.A. Scaife, A.G. Smith, Towards developing algal synthetic biology, *Biochem. Soc. Trans.* 44 (2016) 716–722.
- [12] J.K. Wang, M. Seibert, Prospects for commercial production of diatoms, *Biotechnol. Biofuels* 10 (2017) 16.
- [13] C. Bowler, A.E. Allen, J.H. Badger, J. Grimwood, K. Jabbari, A. Kuo, U. Maheswari, C. Martens, F. Maumus, R.P. Otilar, E. Rayko, A. Salamov, K. Vandepoel, B. Beszteri, A. Gruber, M. Hejide, M. Katinka, T. Mock, K. Valentin, F. Verret, J.A. Berges, C. Brownlee, J.P. Cadoret, A. Chiovitti, C.J. Choi, S. Coesel, A. De Martino, J.C. Detter, C. Durkin, A. Falciatore, J. Fournet, M. Haruta, M.J. Huysman, B.D. Jenkins, K. Jiroutova, R.E. Jorgensen, Y. Joubert, A. Kaplan, N. Kroger, P.G. Kroth, J. La Roche, E. Lindquist, M. Lommer, V. Martin-Jezequel, P.J. Lopez, S. Lucas, M. Mangogna, K. McGinnis, L.K. Medlin, A. Montsant, M.P. Oudot-Le Secq, C. Napoli, M. Obornik, M.S. Parker, J.L. Petit, B.M. Porcel, N. Poulsen, M. Robison, L. Rychlewski, T.A. Ryneerson, J. Schmutz, H. Shapiro, M. Siant, M. Stanley, M.R. Sussman, A.R. Taylor, A. Vardi, P. von Dassow, W. Vyverman, A. Willis, L.S. Wyrwicz, D.S. Rokhsar, J. Weissenbach, E.V. Armbrust, B.R. Green, Y. Van de Peer, I.V. Grigoriev, The phaeodactylum genome reveals the evolutionary history of diatom genomes, *Nature* 456 (2008) 239–244.
- [14] H. Abida, L.J. Dolch, C. Mei, V. Villanova, M. Conte, M.A. Block, G. Finazzi, O. Bastien, L. Tirichine, C. Bowler, F. Rebeille, D. Petroustos, J. Jouhet, E. Marechal, Membrane glycerolipid remodeling triggered by nitrogen and phosphorus starvation in *Phaeodactylum tricornutum*, *Plant Physiol.* 167 (2015) 118–136.
- [15] P.G. Kroth, A.M. Bones, F. Daboussi, M.I. Ferrante, M. Jaubert, M. Kolot, M. Nymark, C. Rio Bartulos, A. Ritter, M.T. Russo, M. Serif, P. Winge, A. Falciatore, Genome editing in diatoms: achievements and goals, *Plant Cell Rep.* 37 (2018) 1401–1408.
- [16] H.M. Nguyen, M. Baudet, S. Cuiñé, J.-M. Adriano, D. Barthe, E. Billon, C. Bruley, F. Beisson, G. Peltier, M. Ferro, Y. Li-Beisson, Proteomic profiling of oil bodies isolated from the unicellular green microalga *Chlamydomonas reinhardtii*: with focus on proteins involved in lipid metabolism, *Proteomics* 11 (2011) 4266–4273.
- [17] J. Popko, C. Herrfurth, K. Feussner, T. Ischebeck, T. Iven, R. Haslam, M. Hamilton, O. Sayanova, J. Napier, I. Khozin-Goldberg, I. Feussner, Metabolome analysis reveals betaine lipids as major source for triglyceride formation, and the accumulation of sedoheptulose during nitrogen-starvation of *Phaeodactylum tricornutum*, *PLoS One* 11 (2016) e0164673.
- [18] S. Yao, A. Brandt, H. Egsgaard, C. Gjermansen, Neutral lipid accumulation at elevated temperature in conditional mutants of two microalgae species, *Plant Physiol. Biochem.* 61 (2012) 71–79.
- [19] A. Alboresi, G. Perin, N. Vitulo, G. Diretto, M. Block, J. Jouhet, A. Meneghesso, G. Valle, G. Giuliano, E. Marechal, T. Morosinotto, Light remodels lipid biosynthesis in *Nannochloropsis gaditana* by modulating carbon partitioning between organelles, *Plant Physiol.* 171 (2016) 2468–2482.
- [20] L.-J. Dolch, J. Lupette, G. Tourcier, M. Bedhomme, S. Collin, L. Magneschi, M. Conte, K. Seddiki, C. Richard, E. Corre, L. Fourage, F. Laeuffer, R. Richards, M. Reith, F. Rébeillé, J. Jouhet, P. McGinn, E. Maréchal, Nitric oxide mediates nitrite-sensing and acclimation and triggers a remodeling of lipids, *Plant Physiol.* 175 (2017) 1407.
- [21] A.R. Burch, A.K. Franz, Combined nitrogen limitation and hydrogen peroxide treatment enhances neutral lipid accumulation in the marine diatom *Phaeodactylum tricornutum*, *Bioresour. Technol.* 219 (2016) 559–565.
- [22] J.R. Collins, B.R. Edwards, H.F. Fredricks, B.A.S. Van Mooy, LOBSTAHS: an adduct-based lipidomics strategy for discovery and identification of oxidative stress biomarkers, *Anal. Chem.* 88 (2016) 7154–7162.
- [23] J. Lupette, Antoine Jaussaud, Claire Vigor, Camille Oger, Jean-Marie Galano, Guillaume Réversat, Joseph Vercauteren, Juliette Jouhet, Thierry Durand, Eric Maréchal, Non-enzymatic synthesis of bioactive isoprostanooids in phaeodactylum following oxidative stress, *Plant Physiol.* 178 (2018) 1344–1357.
- [24] M. Conte, J. Lupette, K. Seddiki, C. Mei, L.-J. Dolch, V. Gros, C. Barette, F. Rébeillé, J. Jouhet, E. Maréchal, Screening for biologically annotated drugs that trigger triacylglycerol accumulation in the diatom phaeodactylum, *Plant Physiol.* 177 (2018) 532.
- [25] N. Wase, P. Black, C. DiRusso, Innovations in improving lipid production: algal chemical genetics, *Prog. Lipid Res.* 71 (2018) 101–123.
- [26] N. Wase, B. Tu, J.W. Allen, P.N. Black, C.C. DiRusso, Identification and metabolite profiling of chemical activators of lipid accumulation in green algae, *Plant Physiol.* 174 (2017) 2146–2165.
- [27] H. Kim, S. Jang, S. Kim, Y. Yamaoka, D. Hong, W.Y. Song, I. Nishida, Y. Li-Beisson, Y. Lee, The small molecule fenpropimorph rapidly converts chloroplast membrane lipids to triacylglycerols in *Chlamydomonas reinhardtii*, *Front. Microbiol.* 6 (2015) 54.
- [28] T.C. Walther, J. Chung, R.V. Farese Jr., Lipid droplet biogenesis, *Annu. Rev. Cell Dev. Biol.* 33 (2017) 491–510.
- [29] C. Zhang, P. Liu, The lipid droplet: a conserved cellular organelle, *Protein Cell* 8 (2017) 796–800.
- [30] D.J. Murphy, The dynamic roles of intracellular lipid droplets: from archaemia to mammals, *Protoplasma* 249 (2012) 541–585.
- [31] D.J. Murphy, The biogenesis and functions of lipid bodies in animals, plants and microorganisms, *Prog. Lipid Res.* 40 (2001) 325–438.
- [32] A. Pol, S.P. Gross, R.G. Parton, Biogenesis of the multifunctional lipid droplet: lipids, proteins, and sites, *J. Cell Biol.* 204 (2014) 635–646.
- [33] F. Wilfling, J.T. Haas, T.C. Walther, R.V.F. Jr, Lipid droplet biogenesis, *Curr. Opin. Cell Biol.* 29 (2014) 39–45.
- [34] W.M. Henne, M.L. Reese, J.M. Goodman, The assembly of lipid droplets and their roles in challenged cells, *EMBO J.* 37 (2018).
- [35] M.H. den Brok, T.K. Raaijmakers, E. Collado-Camps, G.J. Adema, Lipid droplets as immune modulators in myeloid cells, *Trends Immunol.* 39 (2018) 380–392.
- [36] N. Kory, R.V. Farese Jr., T.C. Walther, Targeting fat: mechanisms of protein localization to lipid droplets, *Trends Cell Biol.* 26 (2016) 535–546.
- [37] K.D. Chapman, J.M. Dyer, R.T. Mullen, Biogenesis and functions of lipid droplets in plants: thematic review series: lipid droplet synthesis and metabolism: from yeast to man, *J. Lipid Res.* 53 (2012) 215–226.
- [38] A.H.C. Huang, Plant lipid droplets and their associated proteins: potential for rapid advances, *Plant Physiol.* 176 (2018) 1894–1918.
- [39] H. Itabe, T. Yamaguchi, S. Nimura, N. Sasabe, Perilipins: a diversity of intracellular lipid droplet proteins, *Lipids Health Dis.* 16 (2017) 83.
- [40] E.R. Moellering, C. Benning, RNA interference silencing of a major lipid droplet protein affects lipid droplet size in *Chlamydomonas reinhardtii*, *Eukaryot. Cell* 9 (2010) 97–106.
- [41] G.O. James, C.H. Hocart, W. Hillier, H. Chen, F. Kordbacheh, G.D. Price, M.A. Djordjevic, Fatty acid profiling of *Chlamydomonas reinhardtii* under nitrogen deprivation, *Bioresour. Technol.* 102 (2011) 3343–3351.
- [42] I.P. Lin, P.L. Jiang, C.S. Chen, J.T. Tzen, A unique caleosin serving as the major integral protein in oil bodies isolated from *Chlorella* sp. cells cultured with limited nitrogen, *Plant Physiol. Biochem.* 61 (2012) 80–87.
- [43] E. Peled, S. Leu, A. Zarka, M. Weiss, U. Pick, I. Khozin-Goldberg, S. Boussiba, Isolation of a novel oil globule protein from the green alga *Haematococcus pluvialis* (*Chlorophyceae*), *Lipids* 46 (2011) 851–861.
- [44] L. Davidi, A. Katz, U. Pick, Characterization of major lipid droplet proteins from *Dunaliella*, *Planta* 236 (2012) 19–33.
- [45] A. Javee, S.B. Sulochana, S.J. Palliserry, M. Arumugam, Major lipid body protein: a conserved structural component of lipid body accumulated during abiotic stress in *S. quadricauda* CASA-CC202, *Front. Energy Res.* 4 (2016).
- [46] H. Sieglér, O. Valerius, T. Ischebeck, J. Popko, N.J. Tourasse, O. Vallon, I. Khozin-Goldberg, G.H. Braus, I. Feussner, Analysis of the lipid body proteome of the oleaginous alga *Lobosphaera incisa*, *BMC Plant Biol.* 17 (2017) 98.
- [47] S. Flori, P.-H. Jouneau, G. Finazzi, E. Maréchal, D. Falconet, Ultrastructure of the periplastidial compartment of the diatom *Phaeodactylum tricornutum*, *Protist* 167 (2016) 254–267.
- [48] D. Nojima, T. Yoshino, Y. Maeda, M. Tanaka, M. Nemoto, T. Tanaka, Proteomics analysis of oil body-associated proteins in the oleaginous diatom, *J. Proteome Res.*

- 12 (2013) 5293–5301.
- [49] K. Yoneda, M. Yoshida, I. Suzuki, M.M. Watanabe, Identification of a major lipid droplet protein in a marine diatom *Phaeodactylum tricoratum*, *Plant Cell Physiol.* 57 (2016) 397–406.
- [50] A. Vieler, S.B. Brubaker, B. Vick, C. Benning, A lipid droplet protein of *Nannochloropsis* with functions partially analogous to plant oleosins, *Plant Physiol.* 158 (2012) 1562.
- [51] K. Yoneda, M. Yoshida, I. Suzuki, M.M. Watanabe, Homologous expression of lipid droplet protein-enhanced neutral lipid accumulation in the marine diatom *Phaeodactylum tricoratum*, *J. Appl. Phycol.* 30 (2018) 2793–2802.
- [52] A. Falciatore, M.R. d'Alcalá, P. Croot, C. Bowler, Perception of environmental signals by a marine diatom, *Science* 288 (2000) 2363–2366.
- [53] K.E. Cooksey, J.B. Guckert, S.A. Williams, P.R. Callis, Fluorometric determination of the neutral lipid content of microalgal cells using Nile Red, *J. Microbiol. Methods* 6 (1987) 333–345.
- [54] J. Folch, M. Lees, G.H. Sloane Stanley, A simple method for the isolation and purification of total lipides from animal tissues, *J. Biol. Chem.* 226 (1957) 497–509.
- [55] D. Simionato, M.A. Block, N. La Rocca, J. Jouhet, E. Marechal, G. Finazzi, T. Morosinotto, The response of *Nannochloropsis gaditana* to nitrogen starvation includes de novo biosynthesis of triacylglycerols, a decrease of chloroplast galactolipids, and reorganization of the photosynthetic apparatus, *Eukaryot. Cell* 12 (2013) 665–676.
- [56] G.E. Bligh, W.J. Dyer, A rapid method of total lipid extraction and purification, *Can. J. Biochem. Physiol.* 37 (1959) 911–917.
- [57] J. Jouhet, E. Marechal, R. Bligny, J. Joyard, M.A. Block, Transient increase of phosphatidylcholine in plant cells in response to phosphate deprivation, *FEBS Lett.* 544 (2003) 63–68.
- [58] J. Jouhet, J. Lupette, O. Clerc, L. Magneschi, M. Bedhomme, S. Collin, S. Roy, E. Maréchal, F. Rébeillé, LC-MS/MS versus TLC plus GC methods: consistency of glycerolipid and fatty acid profiles in microalgae and higher plant cells and effect of a nitrogen starvation, *PLoS One* 12 (2017) e0182423.
- [59] B. Deme, C. Cataye, M.A. Block, E. Marechal, J. Jouhet, Contribution of galactoglycerolipids to the 3-dimensional architecture of thylakoids, *FASEB J.* 28 (2014) 3373–3383.
- [60] C.M. Buseman, P. Tamura, A.A. Sparks, E.J. Baughman, S. Maatta, J. Zhao, M.R. Roth, S.W. Esch, J. Shah, T.D. Williams, R. Welti, Wounding stimulates the accumulation of glycerolipids containing oxophytodienoic acid and dinor-oxophytodienoic acid in *Arabidopsis* leaves, *Plant Physiol.* 142 (2006) 28.
- [61] J. Cox, M. Mann, MaxQuant enables high peptide identification rates, individualized p.p.b.-range mass accuracies and proteome-wide protein quantification, *Nat. Biotechnol.* 26 (2008) 1367.
- [62] B. Schwahnhaüsser, D. Busse, N. Li, G. Dittmar, J. Schuchhardt, J. Wolf, W. Chen, M. Selbach, Global quantification of mammalian gene expression control, *Nature* 473 (2011) 337.
- [63] T.N. Petersen, S. Brunak, G. von Heijne, H. Nielsen, SignalP 4.0: discriminating signal peptides from transmembrane regions, *Nat. Methods* 8 (2011) 785–786.
- [64] O. Emanuelsson, H. Nielsen, G. von Heijne, ChloroP, a neural network-based method for predicting chloroplast transit peptides and their cleavage sites, *Protein Sci.* 8 (1999) 978–984.
- [65] A. Gruber, G. Roca, P.G. Kroth, E.V. Armbrust, T. Mock, Plastid proteome prediction for diatoms and other algae with secondary plastids of the red lineage, *Plant J.* 81 (2015) 519–528.
- [66] E.L.L. Sonnhammer, G.V. Heijne, A. Krogh, A hidden markov model for predicting transmembrane helices in protein sequences, *Proceedings of the 6th International Conference on Intelligent Systems for Molecular Biology*, AAAI Press, 1998, pp. 175–182.
- [67] L.P. Kozlowski, IPC – isoelectric point calculator, *Biol. Direct* 11 (2016) 55.
- [68] W.J. Hurkman, C.K. Tanaka, Solubilization of plant membrane proteins for analysis by two-dimensional gel electrophoresis, *Plant Physiol.* 81 (1986) 802.
- [69] S. Flori, P.H. Jouneau, B. Gallet, L.F. Estrozi, C. Morisot, G. Schoehn, G. Finazzi, D. Falconet, Imaging plastids in 2D and 3D: confocal and electron microscopy, *Methods Mol. Biol.* 1829 (2018) 113–122.
- [70] D.L. Brasaemle, T. Barber, N.E. Wolins, G. Serrero, E.J. Blanchette-Mackie, C. Londos, Adipose differentiation-related protein is an ubiquitously expressed lipid storage droplet-associated protein, *J. Lipid Res.* 38 (1997) 2249–2263.
- [71] D.L. Brasaemle, N.E. Wolins, Isolation of lipid droplets from cells by density gradient centrifugation, *Curr. Protoc. Cell Biol.* 72 (2016) 3 15 11–13 15 13.
- [72] S.W. Rampen, B.A. Abbas, S. Schouten, J.S.S. Damste, A comprehensive study of sterols in marine diatoms (Bacillariophyta): implications for their use as tracers for diatom productivity, *Limnol. Oceanogr.* 55 (2010) 91–105.
- [73] M. Fabris, M. Matthijs, S. Carbonelle, T. Moses, J. Pollier, R. Dasseville, G.J. Baart, W. Vyverman, A. Goossens, Tracking the sterol biosynthesis pathway of the diatom *Phaeodactylum tricoratum*, *New Phytol.* 204 (2014) 521–535.
- [74] S. Lopez, B. Bermudez, S. Montserrat-de la Paz, S. Jaramillo, L.M. Varela, A. Ortega-Gomez, R. Abia, F.J. Muriana, Membrane composition and dynamics: a target of bioactive virgin olive oil constituents, *Biochim. Biophys. Acta* 1838 (2014) 1638–1656.
- [75] K. Tauchi-Sato, S. Ozeki, T. Houjou, R. Taguchi, T. Fujimoto, The surface of lipid droplets is a phospholipid monolayer with a unique fatty acid composition, *J. Biol. Chem.* 277 (2002) 44507–44512.
- [76] G. Onal, O. Kutlu, D. Gozuacik, S. Dokmeci Emre, Lipid droplets in health and disease, *Lipids Health Dis.* 16 (2017) 128.
- [77] Z. Yi, M. Xu, M. Magnusdotir, Y. Zhang, S. Brynjolfsson, W. Fu, Photo-oxidative stress-driven mutagenesis and adaptive evolution on the marine diatom *Phaeodactylum tricoratum* for enhanced carotenoid accumulation, *Mar. Drugs* 13 (2015) 6138–6151.
- [78] Y. Lu, X. Wang, S. Balamurugan, W.D. Yang, J.S. Liu, H.P. Dong, H.Y. Li, Identification of a putative seipin ortholog involved in lipid accumulation in marine microalga *Phaeodactylum tricoratum*, *J. Appl. Phycol.* 29 (2017) 2821–2829.
- [79] K.L. Farquharson, Deciphering the role of CGI-58 in lipid metabolism in *Arabidopsis*, *Plant Cell* 25 (2013) 1485.
- [80] S. Park, S.K. Gidda, C.N. James, P.J. Horn, N. Khuu, D.C. Seay, J. Keereetawee, K.D. Chapman, R.T. Mullen, J.M. Dyer, The alpha/beta hydrolase CGI-58 and peroxisomal transport protein PXA1 coregulate lipid homeostasis and signaling in *Arabidopsis*, *Plant Cell* 25 (2013) 1726–1739.
- [81] A. Khatib, Y. Arhab, A. Bentebibel, A. Abousalham, A. Noiri, Reassessing the potential activities of plant CGI-58 protein, *PLoS One* 11 (2016) e0145806.
- [82] D. Moog, S.A. Rensing, J.M. Archibald, U.G. Maier, K.K. Ullrich, Localization and evolution of putative triose phosphate translocators in the diatom *Phaeodactylum tricoratum*, *Genome Biol. Evol.* 7 (2015) 2955–2969.
- [83] Y. Laizet, D. Pontier, R. Mache, M. Kuntz, Subfamily organization and phylogenetic origin of genes encoding plastid lipid-associated proteins of the fibrillin type, *J. Genome Sci. Technol.* 3 (2004) 19–28.
- [84] A. Yousef, Y.H. Laizet, M.A. Block, E. Maréchal, J.-P. Alcaraz, T.R. Larson, D. Pontier, J. Gaffé, M. Kuntz, Plant lipid-associated fibrillin proteins condition jasmonate production under photosynthetic stress, *Plant J.* 61 (2010) 436–445.
- [85] C. Bréhélin, F. Kessler, K.J. van Wijk, Plastoglobules: versatile lipoprotein particles in plastids, *Trends Plant Sci.* 12 (2007) 260–266.
- [86] H.D. Gould, S. Cuine, B. Legeret, Y. Liang, S. Brugiere, P. Auroy, H. Javot, M. Tardif, B. Jones, F. Beisson, G. Peltier, Y. Li-Beisson, Saturating light induces sustained accumulation of oil in plastidial lipid droplets in *Chlamydomonas reinhardtii*, *Plant Physiol.* 171 (2016) 2406–2417.
- [87] T. Moriyama, M. Toyoshima, M. Saito, H. Wada, N. Sato, Revisiting the algal “chloroplast lipid droplet”: the absence of an entity that is unlikely to exist, *Plant Physiol.* 176 (2018) 1519–1530.
- [88] Z. Li, K. Thiel, Peter J. Thul, M. Beller, Ronald P. Kühnlein, Michael A. Welte, Lipid droplets control the maternal histone supply of *Drosophila* embryos, *Curr. Biol.* 22 (2012) 2104–2113.
- [89] D.L. Brasaemle, G. Dolios, L. Shapiro, R. Wang, Proteomic analysis of proteins associated with lipid droplets of basal and lipolytically stimulated 3T3-L1 adipocytes, *J. Biol. Chem.* 279 (2004) 46835–46842.
- [90] A. Gelzinis, V. Butkus, E. Songaila, R. Augulis, A. Gall, C. Buchel, B. Robert, D. Abramavicius, D. Zigmantas, L. Valkunas, Mapping energy transfer channels in fucoxanthin-chlorophyll protein complex, *Biochim. Biophys. Acta* 1847 (2015) 241–247.
- [91] P. Kuczynska, M. Jemiola-Rzeminska, K. Strzalka, Photosynthetic pigments in diatoms, *Mar. Drugs* 13 (2015) 5847–5881.
- [92] J.-C. Huang, F. Chen, G. Sandmann, Stress-related differential expression of multiple  $\beta$ -carotene ketolase genes in the unicellular green alga *Haematococcus pluvialis*, *J. Biotechnol.* 122 (2006) 176–185.
- [93] G. Chen, B. Wang, D. Han, M. Sommerfeld, Y. Lu, F. Chen, Q. Hu, Molecular mechanisms of the coordination between astaxanthin and fatty acid biosynthesis in *Haematococcus pluvialis* (Chlorophyceae), *Plant J.* 81 (2015) 95–107.
- [94] K. Grünewald, J. Hirschberg, C. Hagen, Ketocarotenoid biosynthesis outside of plastids in the unicellular green alga *Haematococcus pluvialis*, *J. Biol. Chem.* 276 (2001) 6023–6029.
- [95] S. Ota, A. Morita, S. Ohnuki, A. Hirata, S. Sekida, K. Okuda, Y. Ohya, S. Kawano, Carotenoid dynamics and lipid droplet containing astaxanthin in response to light in the green alga *Haematococcus pluvialis*, *Sci. Rep.* 8 (2018) 5617.
- [96] T.S. Moore, Phosphatidylcholine synthesis in castor bean endosperm, *Plant Physiol.* 57 (1976) 382–386.
- [97] T.S. Moore, Z. Du, Z. Chen, Membrane lipid biosynthesis in *Chlamydomonas reinhardtii*. In vitro biosynthesis of diacylglyceryltrimethylhomoserine, *Plant Physiol.* 125 (2001) 423–429.
- [98] R. Bartz, W.H. Li, B. Venables, J.K. Zehmer, M.R. Roth, R. Welti, R.G. Anderson, P. Liu, K.D. Chapman, Lipidomics reveals that adiposomes store ether lipids and mediate phospholipid traffic, *J. Lipid Res.* 48 (2007) 837–847.
- [99] K. Grillitsch, M. Connerth, H. Kofeler, T.N. Arrey, B. Rietschel, B. Wagner, M. Karas, G. Daum, Lipid particles/droplets of the yeast *Saccharomyces cerevisiae* revisited: lipidome meets proteome, *Biochim. Biophys. Acta* 1811 (2011) 1165–1176.
- [100] V.A. Ivashov, K. Grillitsch, H. Kofeler, E. Leitner, D. Baeumlisberger, M. Karas, G. Daum, Lipidome and proteome of lipid droplets from the methylotrophic yeast *Pichia pastoris*, *Biochim. Biophys. Acta* 1831 (2013) 282–290.
- [101] C. Botella, E. Sautron, L. Boudiere, M. Michaud, E. Dubots, Y. Yamaryo-Botte, C. Albrieux, E. Marechal, M.A. Block, J. Jouhet, ALA10, a phospholipid flippase, controls FAD2/FAD3 desaturation of phosphatidylcholine in the ER and affects chloroplast lipid composition in *Arabidopsis thaliana*, *Plant Physiol.* 170 (2016) 1300–1314.
- [102] C.Y. Botte, Y. Yamaryo-Botte, T.W. Rupasinghe, K.A. Mullin, J.I. MacRae, T.P. Spurck, M. Kalanon, M.J. Shears, R.L. Coppel, P.K. Crellin, E. Marechal, M.J. McConville, G.I. McFadden, Atypical lipid composition in the purified relict plastid (apicoplast) of malaria parasites, *Proc. Natl. Acad. Sci. U. S. A.* 110 (2013) 7506–7511.
- [103] B.A. Van Mooy, H.F. Fredricks, B.E. Pedler, S.T. Dyhrman, D.M. Karl, M. Koblizek, M.W. Lomas, T.J. Mincer, L.R. Moore, T. Moutin, M.S. Rappe, E.A. Webb, Phytoplankton in the ocean use non-phosphorus lipids in response to phosphorus scarcity, *Nature* 458 (2009) 69–72.
- [104] C. Benning, Z.H. Huang, D.A. Gage, Accumulation of a novel glycolipid and a betaine lipid in cells of *Rhodobacter sphaeroides* grown under phosphate limitation,

- Arch. Biochem. Biophys. 317 (1995) 103–111.
- [105] L.J. Dolch, E. Marechal, Inventory of fatty acid desaturases in the pennate diatom *Phaeodactylum tricoratum*, Mar. Drugs 13 (2015) 1317–1339.
- [106] O. Sayanova, J.A. Napier, Transgenic oilseed crops as an alternative to fish oils, Prostaglandins Leukot. Essent. Fat. Acids 85 (2011) 253–260.
- [107] O. Sayanova, V. Mimouni, L. Ulmann, A. Morant-Manceau, V. Pasquet, B. Schoefs, J.A. Napier, Modulation of lipid biosynthesis by stress in diatoms, Philos. Trans. R. Soc. Lond. Ser. B Biol. Sci. 372 (2017).
- [108] W.R. Riekhof, B.B. Sears, C. Benning, Annotation of genes involved in glycerolipid biosynthesis in *Chlamydomonas reinhardtii*: discovery of the betaine lipid synthase BTA1Cr, Eukaryot. Cell 4 (2005) 242–252.
- [109] H. Murakami, T. Nobusawa, K. Hori, M. Shimojima, H. Ohta, Betaine lipid is crucial for adapting to low temperature and phosphate deficiency in *Nannochloropsis*, Plant Physiol. 177 (2018) 181–193.
- [110] L. Alipanah, J. Rohloff, P. Winge, A.M. Bones, T. Brembu, Whole-cell response to nitrogen deprivation in the diatom *Phaeodactylum tricoratum*, J. Exp. Bot. 66 (2015) 6281–6296.
- [111] O. Levitan, J. Dinamarca, E. Zelzion, D.S. Lun, L.T. Guerra, M.K. Kim, J. Kim, B.A. Van Mooy, D. Bhattacharya, P.G. Falkowski, Remodeling of intermediate metabolism in the diatom *Phaeodactylum tricoratum* under nitrogen stress, Proc. Natl. Acad. Sci. U. S. A. 112 (2015) 412–417.
- [112] R. Beck, M. Rawet, F.T. Wieland, D. Cassel, The COPI system: molecular mechanisms and function, FEBS Lett. 583 (2009) 2701–2709.
- [113] M. Beller, C. Sztalryd, N. Southall, M. Bell, H. Jackle, D.S. Auld, B. Oliver, COPI complex is a regulator of lipid homeostasis, PLoS Biol. 6 (2008) e292.
- [114] W. Wang, S. Wei, L. Li, X. Su, C. Du, F. Li, B. Geng, P. Liu, G. Xu, Proteomic analysis of murine testes lipid droplets, Sci. Rep. 5 (2015) 12070.
- [115] T. Serafini, L. Orci, M. Amherdt, M. Brunner, R.A. Kahn, J.E. Rothman, ADP-ribosylation factor is a subunit of the coat of Golgi-derived COP-coated vesicles: a novel role for a GTP-binding protein, Cell 67 (1991) 239–253.
- [116] F. Wilfling, A.R. Thiam, M.J. Olarte, J. Wang, R. Beck, T.J. Gould, E.S. Allgeyer, F. Pincet, J. Bewersdorf, R.V. Farese Jr., T.C. Walther, Arf1/COPI machinery acts directly on lipid droplets and enables their connection to the ER for protein targeting, eLife 3 (2014) e01607.
- [117] G. Jurgens, Membrane trafficking in plants, Annu. Rev. Cell Dev. Biol. 20 (2004) 481–504.
- [118] Y. Guo, C. Chang, R. Huang, B. Liu, L. Bao, W. Liu, AP1 is essential for generation of autophagosomes from the trans-Golgi network, J. Cell Sci. 125 (2012) 1706–1715.
- [119] K. Soreng, T.P. Neufeld, A. Simonsen, Membrane trafficking in autophagy, Int. Rev. Cell Mol. Biol. 336 (2018) 1–92.
- [120] S. Martens, H.T. McMahon, Mechanisms of membrane fusion: disparate players and common principles, Nat. Rev. Mol. Cell Biol. 9 (2008) 543–556.
- [121] J. Longworth, D. Wu, M. Huete-Ortega, P.C. Wright, S. Vaidyanathan, Proteome response of *Phaeodactylum tricoratum*, during lipid accumulation induced by nitrogen depletion, Algal Res. 18 (2016) 213–224.
- [122] T. Ma, Y.Y. Li, J. Zhu, L.L. Fan, W.D. Du, C.H. Wu, G.P. Sun, J.B. Li, Enhanced autophagic flux by endoplasmic reticulum stress in human hepatocellular carcinoma cells contributes to the maintenance of cell viability, Oncol. Rep. 30 (2013) 433–440.
- [123] B. Pajak, M. Songin, J.B. Strosznajder, A. Orzechowski, B. Gajkowska, Ultrastructural evidence of amyloid beta-induced autophagy in PC12 cells, Folia Neuropathol. 47 (2009) 252–258.
- [124] N. Nelson, N. Perzov, A. Cohen, K. Hagai, V. Padler, H. Nelson, The cellular biology of proton-motive force generation by V-ATPases, J. Exp. Biol. 203 (2000) 89–95.
- [125] Q. Shi, H. Araie, R.K. Bakku, Y. Fukao, R. Rakwal, I. Suzuki, Y. Shiraiwa, Proteomic analysis of lipid body from the alkenone-producing marine haptophyte alga *Tisochrysis lutea*, Proteomics 15 (2015) 4145–4158.
- [126] S. D'Andrea, Lipid droplet mobilization: the different ways to loosen the purse strings, Biochimie 120 (2016) 17–27.
- [127] C. Deruyffelaere, Z. Purkrtova, I. Bouchez, B. Collet, J.L. Cacas, T. Chardot, J.L. Gallois, S. D'Andrea, PUX10 associates with CDC48A and regulates the dislocation of ubiquitinated oleosins from seed lipid droplets, Plant Cell 30 (2018) 2116–2136.
- [128] F.K. Kretzschmar, L.F. Mengel, A. Muller, K. Schmitt, K.F. Biersch, O. Valerius, G. Braus, T. Ischebeck, PUX10 is a lipid droplet-localized scaffold protein that interacts with CDC48 and is involved in the degradation of lipid droplet proteins, Plant Cell 30 (2018) 2137–2160.
- [129] Y. Okuda-Shimizu, L.M. Hendershot, Characterization of an ERAD pathway for nonglycosylated BiP substrates, which require Herp, Mol. Cell 28 (2007) 544–554.
- [130] J. Stevenson, E.Y. Huang, J.A. Olzmann, Endoplasmic reticulum-associated degradation and lipid homeostasis, Annu. Rev. Nutr. 36 (2016) 511–542.
- [131] S. Hatakeyama, M. Yada, M. Matsumoto, N. Ishida, K.-I. Nakayama, U box proteins as a new family of ubiquitin-protein ligases, J. Biol. Chem. 276 (2001) 33111–33120.
- [132] S. Schmollinger, T. Muhlhaus, N.R. Boyle, I.K. Blaby, D. Casero, T. Mettler, J.L. Moseley, J. Kropat, F. Sommer, D. Strenkert, D. Hemme, M. Pellegrini, A.R. Grossman, M. Stitt, M. Schroda, S.S. Merchant, Nitrogen-sparing mechanisms in *Chlamydomonas* affect the transcriptome, the proteome, and photosynthetic metabolism, Plant Cell 26 (2014) 1410–1435.
- [133] J.J. Park, H. Wang, M. Gargouri, R.R. Deshpande, J.N. Skepper, F.O. Holguin, M.T. Juergens, Y. Shachar-Hill, L.M. Hicks, D.R. Gang, The response of *Chlamydomonas reinhardtii* to nitrogen deprivation: a systems biology analysis, Plant J. 81 (2015) 611–624.
- [134] R. Satoh, K. Hagihara, R. Sugiura, Rae1-mediated nuclear export of Rnc1 is an important determinant in controlling MAPK signaling, Curr. Genet. 64 (2018) 103–108.
- [135] S. Cermelli, Y. Guo, S.P. Gross, M.A. Welte, The lipid-droplet proteome reveals that droplets are a protein-storage depot, Curr. Biol. 16 (2006) 1783–1795.
- [136] J.L. Soulages, S.J. Firdaus, S. Hartson, X. Chen, A.D. Howard, E.L. Arrese, Developmental changes in the protein composition of *Manduca sexta* lipid droplets, Insect Biochem. Mol. Biol. 42 (2012) 305–320.
- [137] Y. Yu, T. Li, N. Wu, L. Jiang, X. Ji, H. Huang, The role of lipid droplets in *Mortierella alpina* aging revealed by integrative subcellular and whole-cell proteome analysis, Sci. Rep. 7 (2017) 43896.
- [138] Y. Ding, Y. Wu, R. Zeng, K. Liao, Proteomic profiling of lipid droplet-associated proteins in primary adipocytes of normal and obese mouse, Acta Biochim. Biophys. Sin. 44 (2012) 394–406.
- [139] H.-C. Wan, R.C.N. Melo, Z. Jin, A.M. Dvorak, P.F. Weller, Roles and origins of leukocyte lipid bodies: proteomic and ultrastructural studies, FASEB J. 21 (2007) 167–178.
- [140] S. Larsson, S. Resjö, M.F. Gomez, P. James, C. Holm, Characterization of the lipid droplet proteome of a clonal insulin-producing  $\beta$ -cell line (INS-1 832/13), J. Proteome Res. 11 (2012) 1264–1273.
- [141] X. Yu, L. Ye, H. Zhang, J. Zhao, G. Wang, C. Guo, W. Shang, Ginsenoside Rb1 ameliorates liver fat accumulation by upregulating perilipin expression in adipose tissue of db/db obese mice, J. Ginseng Res. 39 (2015) 199–205.
- [142] M. Beller, D. Riedel, L. Jansch, G. Dieterich, J. Wehland, H. Jackle, R.P. Kühnlein, Characterization of the *Drosophila* lipid droplet subproteome, Mol. Cell. Proteomics 5 (2006) 1082–1094.
- [143] C. Lundin, R. Nordstrom, K. Wagner, C. Windpassinger, H. Andersson, G. von Heijne, I. Nilsson, Membrane topology of the human seipin protein, FEBS Lett. 580 (2006) 2281–2284.
- [144] E.M. Trentacoste, R.P. Shrestha, S.R. Smith, C. Gle, A.C. Hartmann, M. Hildebrand, W.H. Gerwick, Metabolic engineering of lipid catabolism increases microalgal lipid accumulation without compromising growth, Proc. Natl. Acad. Sci. U. S. A. 110 (2013) 19748–19753.
- [145] M. Pyc, Y. Cai, M.S. Greer, O. Yurchenko, K.D. Chapman, J.M. Dyer, R.T. Mullen, Turning over a new leaf in lipid droplet biology, Trends Plant Sci. 22 (2017) 596–609.
- [146] X.L. Li, Y.F. Pan, H.H. Hu, Identification of the triacylglycerol lipase in the chloroplast envelope of the diatom *Phaeodactylum tricoratum*, Algal Research-Biomass Biofuels and Bioproducts, 33 2018, pp. 440–447.
- [147] D. Ewe, M. Tachibana, S. Kikutani, A. Gruber, C. Rio Bartulos, G. Konert, A. Kaplan, Y. Matsuda, P.G. Kroth, The intracellular distribution of inorganic carbon fixing enzymes does not support the presence of a C4 pathway in the diatom *Phaeodactylum tricoratum*, Photosynth. Res. 137 (2018) 263–280.